A TUTORIAL ON SMALL-ANGLE NEUTRON SCATTERING FROM POLYMERS

Boualem Hammouda

National Institute of Standards and Technology
Materials Science and Engineering Laboratory
Building 235, Room E151
Gaithersburg, MD 20899

June 1995

I. INTRODUCTION

Neutron scattering has found wide use for the characterization of polymers owing to the partial deuteration method. Use of deuterated macromolecules in a non-deuterated environment is comparable to the staining method used in electron microscopy in order to enhance contrast. Polymer science and neutron scattering have been recognized at the highest level, through the award of the Nobel Prize in Physics to P.G. de Gennes in 1991 and to C. Schull and B. Brockhouse in 1994.

Small-angle neutron scattering (SANS) is a well-established characterization method for microstructure investigations in various materials. It can probe inhomogeneities from the near atomic scale (1nm) to the near micron scale (600nm). Since the construction of the first SANS instrument over 25 years ago, this technique has experienced a steady growth with over 20 instruments constructed worldwide. These are either reactor-based instruments using monochromated neutron beams or time-of-flight instruments at pulsed neutron sources. SANS has had major impact on the understanding of polymer conformations, morphology, rheology, thermodynamics, etc. This technique has actually become a "routine" analytic characterization method even for the non-experts.

These notes are intended to help first time users of neutron scattering acquire (or brush up on) basic knowledge on the technique, and on its applications to polymer systems. Because the focus will be on small-angle neutron scattering, quasielastic/inelastic scattering and the dynamics of polymers will not be discussed. Neutron production, SANS instrumentation and structure factor calculations have been included along with elementary modeling methods for homogeneous polymer mixtures as well as phase separated systems (domain scattering). Readers of these notes need not be experts in nuclear physics, statistical mechanics or advanced mathematics; basic knowledge in such areas is, of course, useful. Also knowledge of the Fourier transform method is essential for understanding reciprocal space.

After a brief review of basic neutron properties, we will introduce the major processes used to produce neutrons as well as list the major neutron sources in the United States and in the world. Production of cold neutrons (essential for SANS applications) is discussed along with description of cold neutron remoderators. SANS instrumentation is then examined in no great detail focussing on the major components and pointing out differences between reactor-based and spallation source-based instruments. Elements of neutron scattering in general will follow; including advantages and disadvantages of the technique, scattering lengths and cross sections, coherent/incoherent scattering contributions, and example calculations. Because "most SANS spectra look alike", SANS is a heavily model-dependent method. Models of single-particle structure factors are discussed with no attempt at completeness. Interparticle contributions are introduced for both homogeneous polymer mixtures (solutions, blends, etc) and phase separated systems (microphase separated copolymers for example) using two simple models (random phase approximation and Ornstein-Zernike equation). The first few chapters (I-VII) are general enough to benefit everyone interested in the SANS technique, the remaining chapters focus on SANS from polymers. Those interested in biopolymers and microemulsions would also benefit from these last chapters. The last few chapters (VIII-XII) concentrate on polymer systems. Data borrowed from research projects of this author are included. Because this is a tutorial and not an extensive review article, the focus is on simple issues and only representative data are discussed.

References to published material in the subject (especially review articles and books) are included along with "Questions" that are meant to help the reader think about some extra issues.

Even though the focus of the notes is on polymer materials, knowledge acquired can be useful to understand scattering from other systems. The field of polymers is at the top of the users list for

SANS (40% of the users at NIST), followed by complex fluids (24% at NIST) and biology (14%). Modeling of these systems, for instance, involves two main parts to the scattering function describing intra-"particle" and interparticle contributions. The word "particle" is often used to refer to scattering inhomogeneities such as deuterated polymer chains, domains in microphase separated copolymers, micelles in microemulsions, latex spheres in colloidal suspensions, etc. The modeling will be kept at its basic level for the sake of simplicity; structure factors for many particle shapes (spherical, rodlike, etc) and many chain architectures are available. Interparticle structure factors based on the Ornstein-Zernike equation for uniform density objects or the mean field random phase approximation for polymer mixtures are also briefly described.

Because polarized neutron beams have not found applications in polymer research, polarization capabilities on SANS instruments will not be discussed. Deuterium is known to effect changes in sample properties (documented shifts of phase transition lines by a few degrees in polymer systems for example); Because they are small, these effects will also not be discussed.

II. BASIC PROPERTIES OF THE NEUTRON

The neutron was discovered by Chadwick in 1932. It has zero charge, a mass of 1.0087 atomic mass unit, a spin of 1/2 and a magnetic moment of -1.9132 nuclear magnetons. It has a half life of 894 seconds and decays into a proton, an electron and an antineutrino. Its interactions with matter are confined to the short-range nuclear and magnetic interactions. Since its interaction probability is small, the neutron usually penetrates well through matter making it a unique probe for investigating bulk condensed matter. Since the neutron can be reflected by some surfaces when incident at glancing angles, it can also be used as a surface probe. Neutrons are scattered by nuclei in samples or by the magnetic moments associated with unpaired electron spins (dipoles) in magnetic samples. Because the nuclear scattering potential is short range, neutron scattering can be described by "s wave" scattering so that the scattering cross section can be described by the first Born approximation.

Some useful relations follow:

Mass: $m = 1.675 \times 10^{-24}$ gm

Magnetic Moment: $\mu_n = 6.031 \times 10^{-12}$ eV/gauss

Energy: $E[meV] = 2.072\ k^2\ [A^{-2}] = 4.135\ f\ [THz] = 0.658\ \omega\ [THz]$
$= 81.787/\lambda^2\ [A^{-2}] = 5.228 \times 10^{-6}\ v^2\ [m^2/sec^2]$
$= 0.0862\ T\ [^oK]$

Wavelength: λ [A] = 3955/v [m/sec]; Velocity: v = 1m/msec (at λ=4A)

k: wavenumber
f: frequency
ω: pulsation (=f/2π)
T: temperature.

III. NEUTRON SOURCES

Since the early days of neutron scattering, there has been an insatiable demand for higher and higher neutron fluxes. Neutron sources are based on various processes that liberate excess neutrons in neutron rich nuclei such as Be, W, U, Ta or Pb. Presently, the highest fluxes available are around a few $x10^{15}$ n/cm^2sec. Even though various neutron sources exist, only a few are actually useful for scattering purposes. These are:

-- continuous reactors
-- spallation sources
-- pulsed reactors and fission boosters.
-- photoneutron sources

Emphasis will be put here on continuous reactors and spallation sources. Only minor improvements in flux increase of continuous reactors are expected because of the saturation of the technology (i.e., limit of heat removal rate and operating safety considerations). Pulsed sources are expected to go to higher fluxes (non-continuous operation allows for a better heat removal rate). Nuclear weapons are ultimate neutron sources delivering 10^{29} neutrons/kiloton in 1 μsec but are unpractical to use for scattering purposes (!).

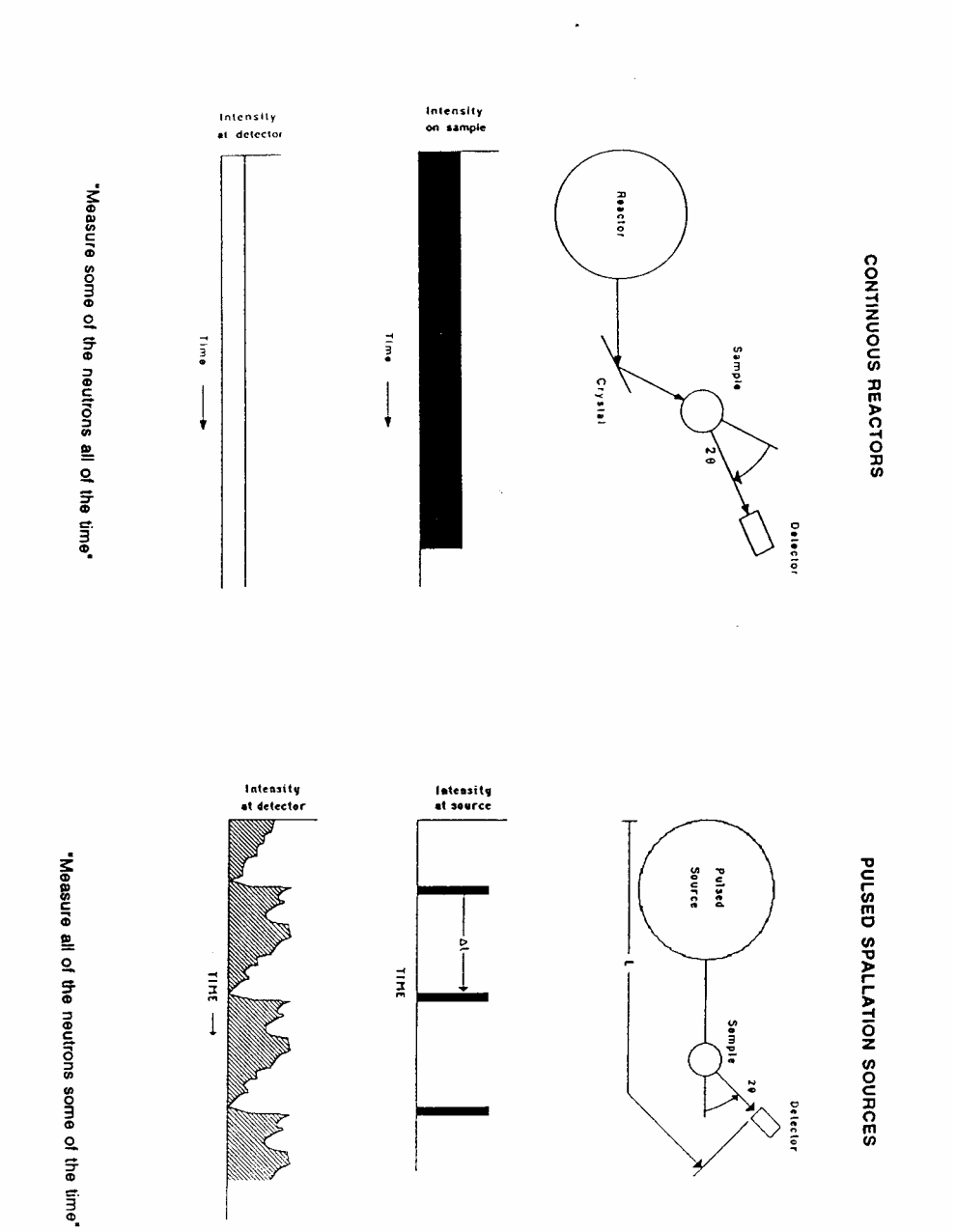

Figure III.1: The two main neutron sources: continuous reactors and pulsed sources. Using continuous reactors, one measures "some of the neutrons all of the time" while with pulsed sources, one measures "all of the neutrons some of the time".

III. 1. Nuclear Fission Reactions

Some heavy nuclides fission into lighter ones (called fission products) upon absorption of a neutron. Known fissile nuclides are U-233, U-235, Pu-239 and Pu-241, but the most used ones are U-235 and Pu-239. Each fission event releases huge energies (200MeV) in the form of kinetic energy of the fission fragments, gamma rays and several fast neutrons. Fission fragments are heavy and remain inside the fuel elements therefore producing the major source of heat while energetic gammas and fast neutrons penetrate most everything and are carefully shielded against. Gamma rays and fast neutrons are a nuisance to neutron scatterers and are not allowed to reach the detectors as much as possible. After being slowed down by the moderator material (usually light or heavy water) neutrons are used to sustain the fission reaction as well as in beam tubes for low energy neutron scattering.

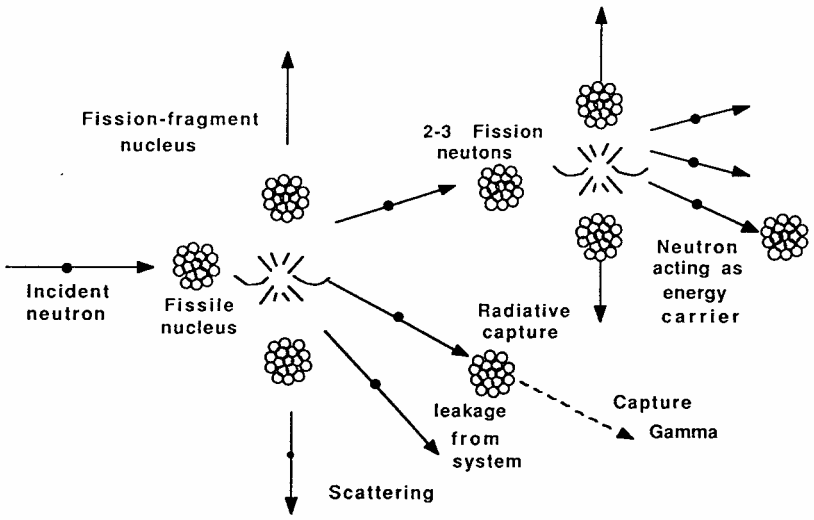

Figure III. 2: Typical fission chain reaction.

III. 2. Nuclear Reactors

Nuclear reactors are based on the fission reaction of U-235 (mainly) to yield 2-3 neutrons/fission at 2MeV kinetic energies. Moderators (D_2O, H_2O) are used to slow down the neutrons to thermal (0.025eV) energies. Reflectors (D_2O, Be, graphite) are used to maintain the core critical. Whereas electrical power producing reactors use wide core sizes and low fuel enrichment (2-3% U-235), research reactors use compact cores and highly enriched fuel (over 90%) in order to achieve high neutron fluences. Regulatory agencies encourage the use of intermediate enrichment (20-50%) fuel in order to avoid proliferation of weapon-grade material.

Nuclear research reactors have benefited from technological advances from power producing reactors as well as nuclear submarines (compact cores operating with highly enriched fuel and foolproof safety control systems). The most popular of the present generation of reactors, the pressurized water reactor (PWR), operates at high pressure (70 to 150 bars) in order to achieve high operating temperatures while maintaining the water in its liquid phase.

Neutrons that are produced by fission (2MeV) can either slow down to epithermal then thermal energies, be absorbed by radiative capture, or leak out of the system. The slowing down process is maintained through collisions with low Z material (mostly water is used both as moderator and coolant) while neutron leakage is minimized by surrounding the core by a reflector (also low Z material) blanket. Most of the fission neutrons appear instantaneously (within 10^{-14} sec of the fission event); these are called prompt neutrons. However, less than 1% of the neutrons appear with an appreciable delay time from the subsequent decay of radioactive fission products. Although the delayed neutrons are a very small fraction of the neutron population, these are vital to the operation of nuclear reactors and to the effective control of the nuclear chain reaction by "slowing" the transient kinetics. Without them, a nuclear reactor would respond so quickly that it could not be controlled.

A short list of research reactors in the USA used for neutron scattering follows: HFIR-Oak Ridge National Laboratory (100 MW), HFBR-Brookhaven National Laboratory (60 MW), NIST-The National Institute of Standards and Technology (20 MW), MURR-The University of Missouri (10 MW). These reactors were built during the1960's. The next generation reactor (the Advanced Neutron Source) under planning for ten years at Oak Ridge National Laboratory has been cancelled due to lack of funds.

A short list of research reactors in the world follows: CRNL-Chalk River, Canada (135 MW), IAE-Beijing, China (125 MW), DRHUVA-Bombay, India (100 MW), ILL-Grenoble, France (57 MW), NLHEP-Tsukuba, Japan (50 MW), NERF-Petten, The Netherlands (45 MW), Bhabha ARC-Bombay, India (40 MW), IFF-Julich, Germany (23 MW), JRR3-Tokai Mura, Japan (20 MW), KFKI-Budapest, Hungary (15 MW), HWRR-Chengdo, China (15 MW), LLB-Saclay, France (14 MW), HMI-Berlin, Germany (10 MW), Riso-Roskilde, Denmark (10 MW), VVR-M Leningrad, Russia (10 MW). The ILL-Grenoble facility is the world leader in neutron scattering after two major upgrades over the last 20 years.

Most of these facilities either have or are planning to add a cold source in order to enhance the population of slow neutrons and therefore allow effective use of SANS instruments.

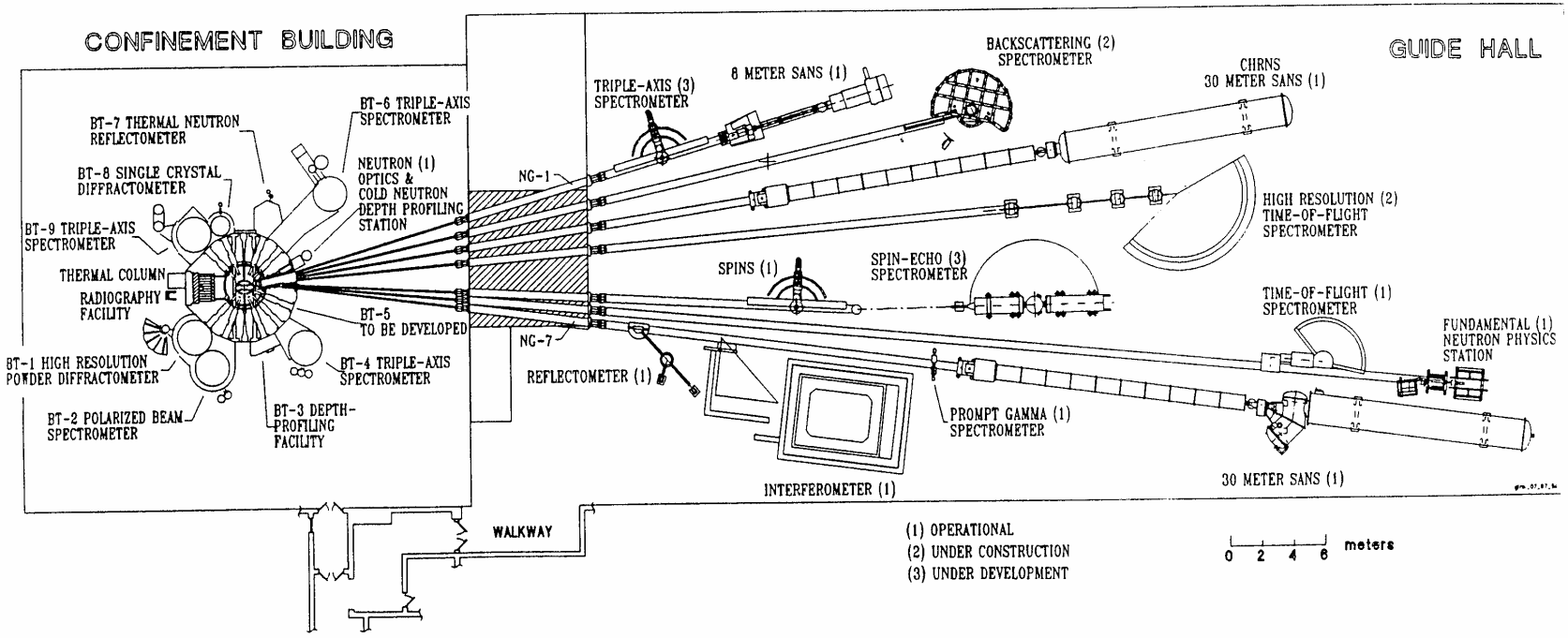
CONFINEMENT BUILDING
GUIDE HALL
BT-7 THERMAL NEUTRON REFLECTOMETER
BT-6 TRIPLE-AXIS SPECTROMETER
BT-8 SINGLE CRYSTAL DIFFRACTOMETER
NEUTRON (1) OPTICS & COLD NEUTRON DEPTH PROFILING STATION
BT-9 TRIPLE-AXIS SPECTROMETER
THERMAL COLUMN
RADIOGRAPHY FACILITY
BT-5 TO BE DEVELOPED
BT-1 HIGH RESOLUTION POWDER DIFFRACTOMETER
BT-4 TRIPLE-AXIS SPECTROMETER
BT-2 POLARIZED BEAM SPECTROMETER
BT-3 DEPTH-PROFILING FACILITY
WALKWAY
NG-1
NG-7
TRIPLE-AXIS (3) SPECTROMETER
8 METER SANS (1)
BACKSCATTERING (2) SPECTROMETER
CHRNS 30 METER SANS (1)
HIGH RESOLUTION (2) TIME-OF-FLIGHT SPECTROMETER
SPINS (1)
SPIN-ECHO (3) SPECTROMETER
TIME-OF-FLIGHT (1) SPECTROMETER
FUNDAMENTAL (1) NEUTRON PHYSICS STATION
REFLECTOMETER (1)
PROMPT GAMMA (1) SPECTROMETER
INTERFEROMETER (1)
30 METER SANS (1)
(1) OPERATIONAL
(2) UNDER CONSTRUCTION
(3) UNDER DEVELOPMENT
0 2 4 6 meters

Figure III.3: Schematics of the NIST reactor and guide hall. Note the two 30 m SANS instruments on the NG3 and NG7 guides and the 8 m instrument on the NG1 guide.

III. 3. Spallation Sources

Beams of high kinetic energy (typically 70MeV) H^- ions are produced (linear accelerator) and injected into a synchrotron ring to reach much higher energies (500-800MeV) and then steered to hit a high Z (neutron rich) target (W-183 or U-238) and produce about 10-30 neutrons/proton with energies about 1MeV. These neutrons are then moderated, reflected, contained, etc., as is usually done in a nuclear reactor. Most spallation sources operate in a pulsed mode. The spallation process produces relatively few gamma rays but the spectrum is rich in high energy neutrons. Typical fast neutron fluxes are 10^{15}-10^{16} n/sec with a 50MeV energy deposition/neutron produced. Booster targets (enriched in U-235) give even higher neutron fluxes.

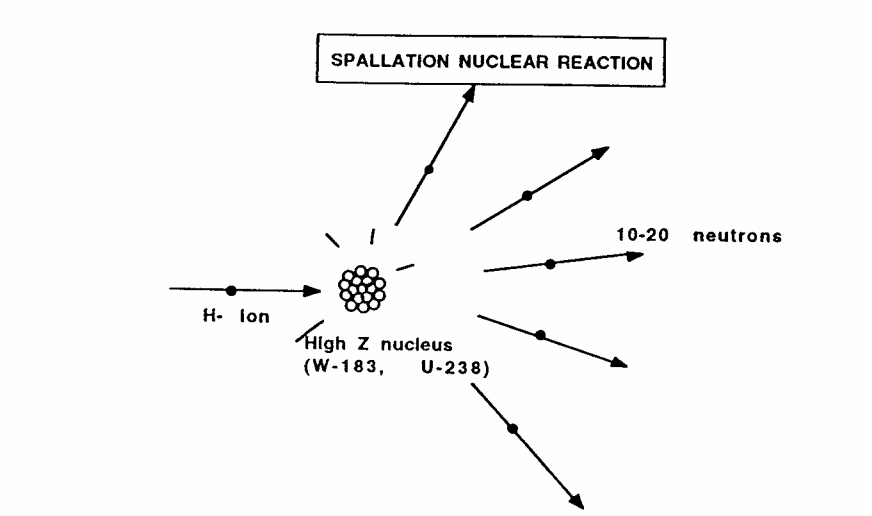

Figure III.4: Spallation Nuclear Reaction.

Major Spallation Sources in the world:

-- IPNS (Argonne): 500MeV protons, U target, 12 μA (30 Hz), pulse width = 0.1μsec, flux = 1.5 x 10^{15} n/sec, operating since 1981.

-- SNS (Rutherford, UK): 800MeV protons, U target, 200 μA (50 Hz), pulse width = 0.27μsec, flux = 4 x 10^{16} n/sec, operating since 1984.

-- WNR/PSR LANSCE (Los Alamos): 800MeV protons, W target, 100 μA (12 Hz), pulse width = 0.27μsec, flux = 1.5 x10^{16} n/sec, operating since 1986.

-- KENS (Tsukuba, Japan): 500MeV protons, U target,100 μA (12 Hz), pulse width = 0.07μsec, flux = 3 x 10^{14} n/sec, operating since 1980.

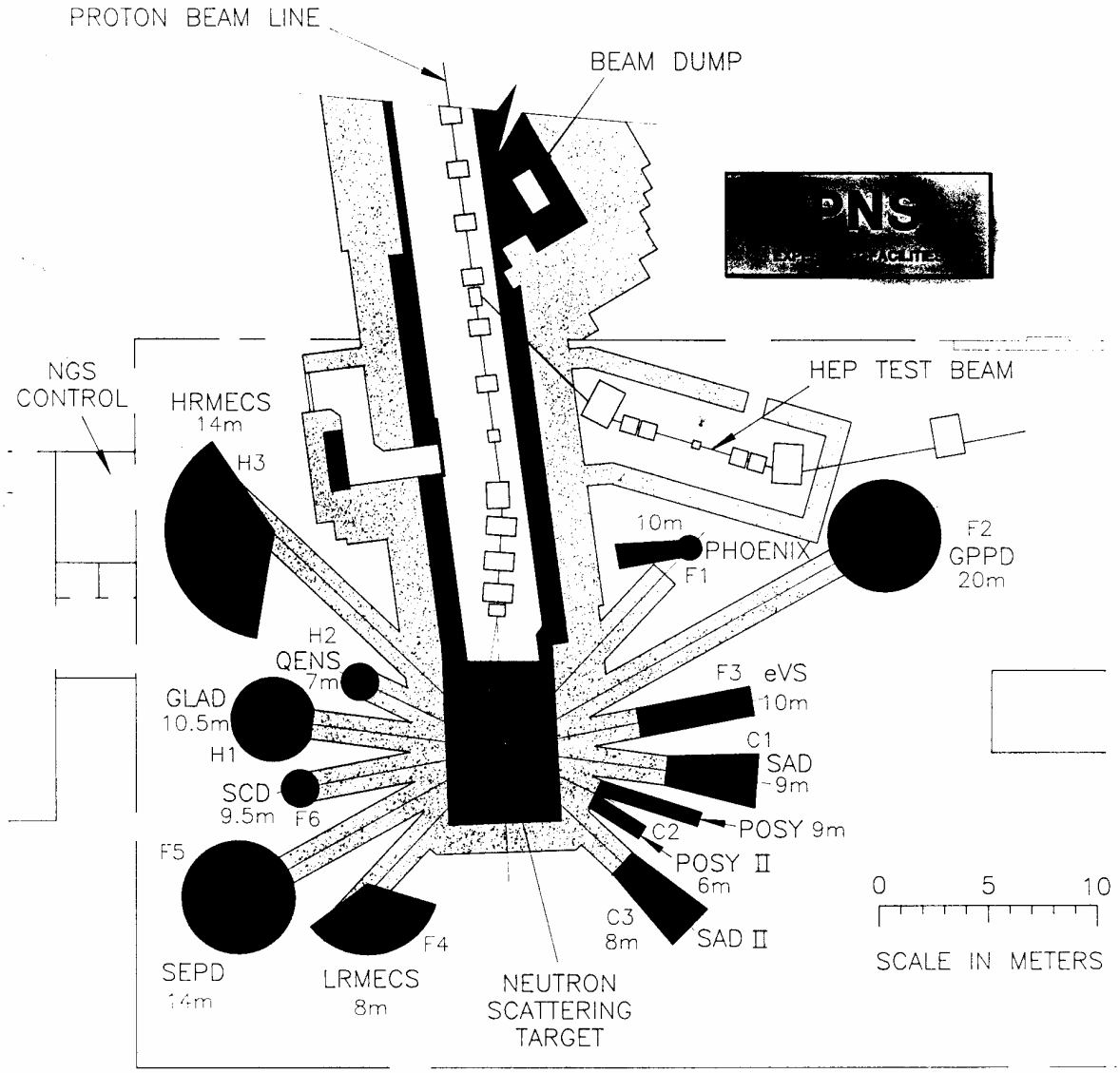

Figure III.5: Schematic of the IPNS spallation source and instruments hall. Note the two SANS instruments (SAD and SADII).

III. 4. Pulsed Reactors

Pulsed reactors include a moving element of fuel (or reflector material which periodically passes near the core), causing brief variation of the reactivity. A fast rising burst of neutrons occurs when the reactivity exceeds prompt critical. One such reactors exists at IBR-30 (Dubna, USSR), with 0.03 MW power, pulse width of 50μsec, repetition rate of 5 Hz. Neutron fluxes are of order 5 x 10^{15} n/cm^{2}sec.

III. 5. Photoneutron Sources

Photoneutron sources are based on the production of evaporation neutrons by photonuclear reactions or by photofission. The photons used (gammas) are produced by electron Bremsstrahlung (photons emitted when electrons are decelerated) in high Z targets (W, U or Ta). The high Z target (W, U or Ta) acts as both the medium that slows down the electrons (therefore producing gammas) and the neutron emitting element (through photonuclear reactions). One such neutron source existed at the Linac I at Harwell (not operating anymore) with 140MeV e^- on Ta target which produced 10^{13} n/sec. Energy deposition is about 2000MeV/neutron produced. This source was characterized by a high gamma-ray background.

References

L.R. Lamarsh, "Introduction to Nuclear Engineering", Addison Wesley Pub. Co., (1977).

J.J. Duderstadt and L.J. Hamilton, "Nuclear Reactor Analysis", J. Wiley and Sons, Inc., (1976).

J.M. Carpenter and W.B. Yelon, "Neutron Sources", Methods of Experimental Physics 23A, 99-196 (1986).

NIST Annual Reports, National Institute of Standards and Technology, 1989-1994.

IPNS Progress Reports, Argonne National Lab, 1983-1993.

G.H. Lander and V.J. Emery, "Scientific Opportunities with Advanced Facilities for Neutron Scattering", Nucl. Inst. and Methods B12, 525 (1985).

KENS Report VI, National Lab for High Energy Physics, KER Japan, 1985-1986.

J. Baruchel, J.L. Hodeau, M.S. Lehmann, J.R. Regnard and C. Schlenker, "Neutron and Synchrotron Radiation for Condensed Matter Studies", Vol 1, Theory, Instruments and Methods, Springer-Verlag (1993).

III. 6. Questions

1. Find out when was the first research reactor built?
2. Name a few applications of nuclear research reactors besides neutron scattering.
3. Do research reactors produce electrical power?
4. What is the origin of delayed neutrons?
5. Are there nuclear reactors that use non-enriched Uranium?
6. Name the research reactor and the spallation source closest to your home institution.
7. Instruments at pulsed sources use a range of wavelengths whereas reactor-based instruments use single wavelength. How could the same scattering information be obtained from these two different types of instruments?
8. Why are most SANS instruments installed in neutron guide halls?
9. What is the cost of running a research reactor? a spallation source?
10. What is a dosimeter?

IV. COLD NEUTRON REMODERATORS

IV. 1. Cold Neutron Source

"Cold" (slow) neutrons are often needed for better spatial resolution in scattering applications (long wavelength scattering). Atoms with low Z (such as H or D) are good moderators making them ideal as cold source material. Cold neutrons are generated in a neutron remoderator also called "cold source" using either hydrogen or deuterium in the liquid form, supercooled gas form, or solid form (methane or ice). The Maxwellian neutron spectral distribution (peaking at 1.8 A for thermal neutrons) is shifted to lower energies by neutron slowing down (through inelastic scattering) processes. The mean free path (average distance between collisions) of neutrons in hydrogen (0.43 cm) is smaller than in deuterium (2.52 cm).

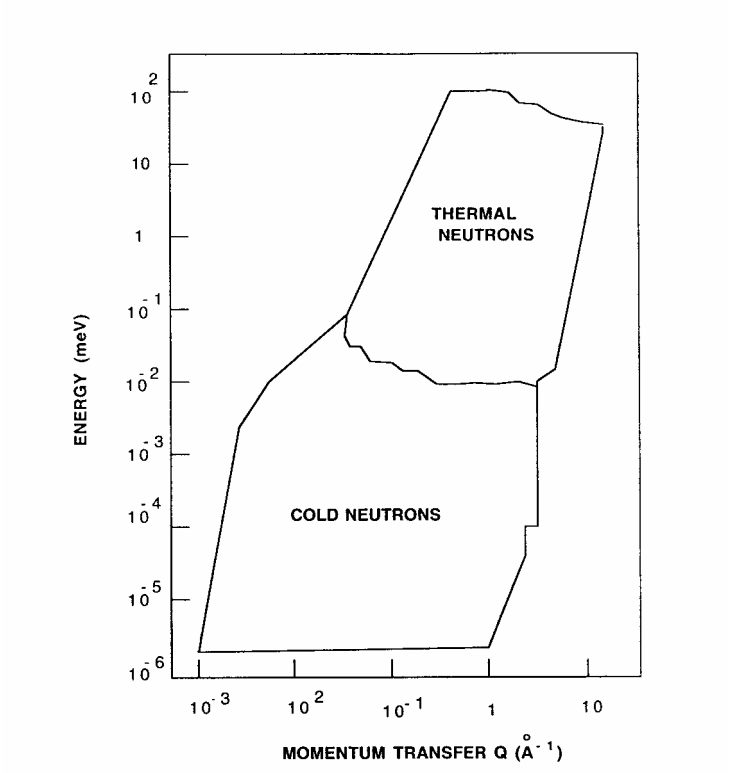

Figure IV.1: Cold neutrons are needed for structural and dynamics studies.

Liquid cold sources (hydrogen or deuterium) operate at low temperature (around 20 K) and 2 bar pressure. Vacuum and helium jackets isolate the remoderating liquid from the surrounding. Supercritical gas cold sources (hydrogen or deuterium) operate at 40 K and 15 bars of pressure (one phase system); thicker walls are necessary for the containment of the higher gas pressure. Solid methane at 50 K and solid ice at 35 K have been used as cold source material. Radiation damage in solid state cold sources produces stored (so called "Wigner") energy due to ionization. In order to avoid sudden release of this energy (explosion!), a recombination of radiolysis products is induced in the cold source material by warming it up on a regular basis (once every a couple of days).

Use of a cold source yields high gains (one to two orders of magnitude) at high wavelengths.

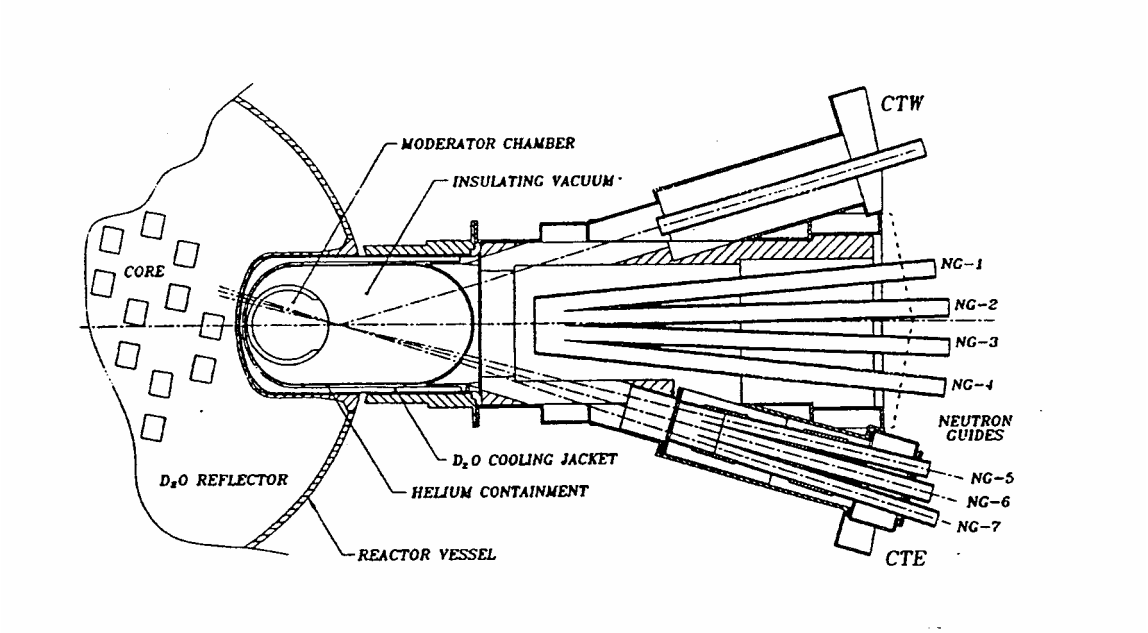

Figure IV. 2: The NIST liquid hydrogen cold source and guide system.

Table IV.1: Cold Neutron Sources in the World

Place	Source	Power	Moderator	Dates
Bombay, India	DHRUVA	100 MW	liq CH_4	1986
Brookhaven, USA	HFBR	60 MW	liq H_2	1977
Grenoble, France	RHF/ILL	57 MW	liquid D	1972,85,87
Julich, Germany	FRJ 2	23 MW	liq H_2	1972,85,87
Gaithersburg, USA	NIST	20 MW	sol D_2O, liq H_2	1987,95
Tokai Mura, Japan	JRR-3	20 MW	liq H_2	1988
Budapest, Hungary	KFKI	15 MW	liq H_2	1989
Chengdo, China	HWRR	15 MW	liq H_2	1988
Saclay, France	ORPHEE/LLB	14 MW	liq H_2	1980
Leningrad, Russia	VVR-M	10 MW	liq H_2+liq D_2	1985
Berlin, Germany	BER 2	10 MW	gas H_2	1988
Riso, Denmark	Pluto	10 MW	gas H_2	1975
Rutherford, GB	ISIS	Pulsed	gas H_2,liq CH_4	1985
Argonne, USA	IPNS	Pulsed	sol, liq CH_4	1986
Los Alamos, USA	LANSCE	Pulsed	liq H_2	1986
Tsukuba, Japan	KENS-1	Pulsed	sol CH_4	1987

IV. 2. Cold Neutron Spectrum

Neutrons are produced by fission with energies around 2MeV, then they slow down to form a Maxwellian spectrum distribution which is peaked around the moderator temperature k_BT (in energy units).

The neutron flux $\phi(E)$ is the number of neutrons crossing a unit area ($1cm^2$) per second in all directions and with energies E.

$$\phi(E) = [\phi_o/(k_B T)^2]\, E \exp(-E/k_B T) .$$

Its integral is the total flux:

$$\phi_o = \int_0^\infty dE\, \phi(E) .$$

$\phi(E)$ can also be expressed in terms of the neutron wavelength $\lambda = h/(2mE)^{1/2}$ as:

$$\phi(\lambda) = \phi_o\, [h^4/2(k_B T m)^2](1/\lambda^5) \exp[(-h^2/2mk_B T)(1/\lambda^2)]$$

where h is Planck's constant. For high λ, the flux decreases as $1/\lambda^5$. A cold source effectively shifts the Maxwellian peak to higher wavelengths therefore increasing the population of cold neutrons and yielding better small-angle neutron scattering resolution. For elastic scattering, this means the ability to resolve larger macromolecular structures (close to micron size).

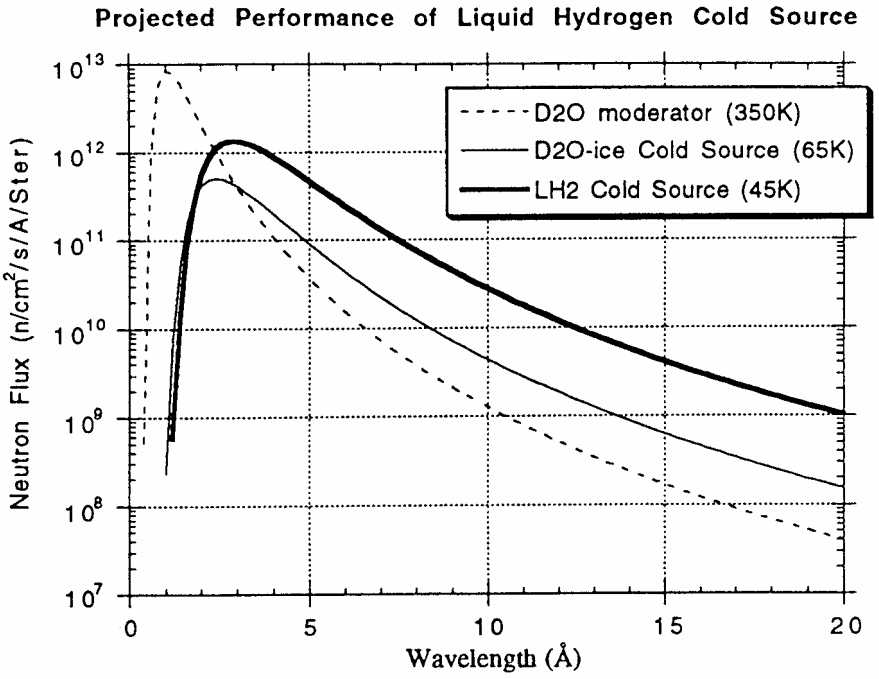

Figure IV. 3: Spectral neutron distributions with and without cold source.

References

A K. Jensen and J.A. Leth, "The Cold Neutron Source in DR_3", Riso National Lab Report M2246 (1980).

R.S. Carter and P.A. Kopetka, "Final Safety Analysis Report on the Heavy Water Neutron Source for the NBS Reactor", Report NBSR-13 (1987).

S.Ikeda and J.M. Carpenter, Nucl. Instr. Meth. A239, 536 (1985).

V. SMALL ANGLE NEUTRON SCATTERING INSTRUMENT

The first SANS instruments utilizing long flight paths, long wavelength neutrons from a reactor cold source and position sensitive detectors were developed in Europe (Julich, Grenoble, Pisa). Small angle neutron scattering instruments should really be called low-Q instruments (Q being the momentum transfer which for low scattering angles θ is given in terms of the neutron wavelength λ as $Q=2\pi\theta/\lambda$). Low Q can be realized either through the use of small angles or high wavelengths. In order to obtain small angles, good collimation and good area detector resolution are needed. Good collimation is achieved through the use of long neutron flight paths before and after the sample. SANS instruments on continuous neutron sources use velocity selectors to

select a slice of the (often cold) neutron spectrum while time of flight SANS instruments use the whole spectral distribution with careful timing between the source chopper and the detector to separate out the various wavelength frames. In this last case (TOF instruments) the maximum length of an instrument is determined by the pulse frequency so as to avoid frame overlap problems (the slowest neutrons of a pulse should not interfere with the fastest neutrons of the next pulse).

V. 1. Continuous SANS Instrument Components

A brief description of the main components of reactor-based SANS instruments follows:

-- Cold neutrons are transported through total internal reflection at glancing angles inside neutron guides. These transmit neutrons from the cold source to the entrance of scattering instruments with little loss.

-- Beam filters (for example, Be for neutrons and Bi for gammas) are used to clean up the beam from unwanted epithermal neutrons (Be transmits neutrons with wavelengths > 4 A) and gamma radiation (stopped by high-Z materials as Bi). Note that if a curved guide is used, no filter is needed because there is no direct line-of-sight from the reactor core (no gammas in the beam) and curved guides transmit only wavelengths above a cutoff wavelength (no epithermal neutrons in the beam). Typical filter thickness is between 15 cm and 20 cm. For better effectiveness, filters are cooled down to liquid nitrogen temperature.

-- A velocity selector yields a monochromatic beam (with wavelengths λ between 4 A and 20 A and wavelength spreads from $\Delta\lambda/\lambda$=10% to 30%). Some SANS instruments that need sharp wavelength resolution use crystal monochromators (with wide mosaic spreads to give $\Delta\lambda/\lambda$<10%) instead. Because $\Delta\lambda/\lambda$ is constant, the neutron spectrum transmitted by the velocity selector falls off as $1/\lambda^4$ (instead of the $1/\lambda^5$ coming from the moderator Maxwellian distribution).

-- An evacuated pre-sample flight path contains a beam collimation system. Typical adjustable flight path distances are from 1 m to 20 m depending on resolution and intensity design considerations. The collimation usually consists of a set of pinholes (source and sample apertures) that converge on the detector. Inside the pre-sample flight path, more neutron guides (with reflecting inner surfaces) are sometime included in parallel with the collimation system for easy insertion into the beam. This allows a useful way to adjust the desired flux on sample along with the desired instrumental resolution by varying the effective source-to-sample distance.

-- A sample chamber usually contains a translation frame that can hold many samples (measured in sequence). Heating and cooling of samples (-150^{o}C to 200^{o}C) as well as other sample environments (cryostats, electromagnets, ovens, shearing devices, etc) are often accomodated.

-- The post sample flight path is usually an evacuated cylindrical tube (to avoid scattering from nitrogen in air) that permits the translation of an area detector along rails in order to change to sample-to-detector distance.

-- The area detector is often a gas detector with 0.5 cm to 1cm resolution and typically 128x128 cells. The detection electronics chain starts with preamplifiers on the back of the detector and comprises amplifiers, coincidence and timing units, plus encoding modules and a means of histogramming the data and mapping them onto computer memory. In order to avoid extensive use of vacuum feedthroughs, the high count rate ILL-type area detector design incorporates most electronics modules (amplification, coincidence, encoding, etc) inside an electronics chamber

that is located on the back of the detector. In this design, flexible hoses are, however, needed to ventilate the electronics and to carry the HV cable in and the encoded signal out.

-- A set of beam stops is used to prevent the main beam from reaching the detector and therefore damaging it due to overexposure. Use of Li-6 glass as neutron absorber avoids the gamma-ray background obtained with Cd, B or Gd containing materials. For easy alignment, motion of the beam stops should be independent of that of the area detector.

-- A low-efficiency fission chamber detector located right after the velocity selector is used to monitor the neutron beam during data acquisition and a He-3 thin pencil detector is mounted on one of the beam stops (that can be moved in or out of the beam) for transmission measurements.

-- Gamma radiation produced by neutron capture in various neutron absorbing materials (Cd, Gd, B) is stopped using high-Z shield materials (Fe, Pb, concrete). Shields surround the velocity selector and beam defining apertures. The scattering vessel is also shielded in order to minimize background reaching the detector.

-- Data acquisition is computer controlled within menu-driven screen management environments and on-line imaging of the data is usually available.

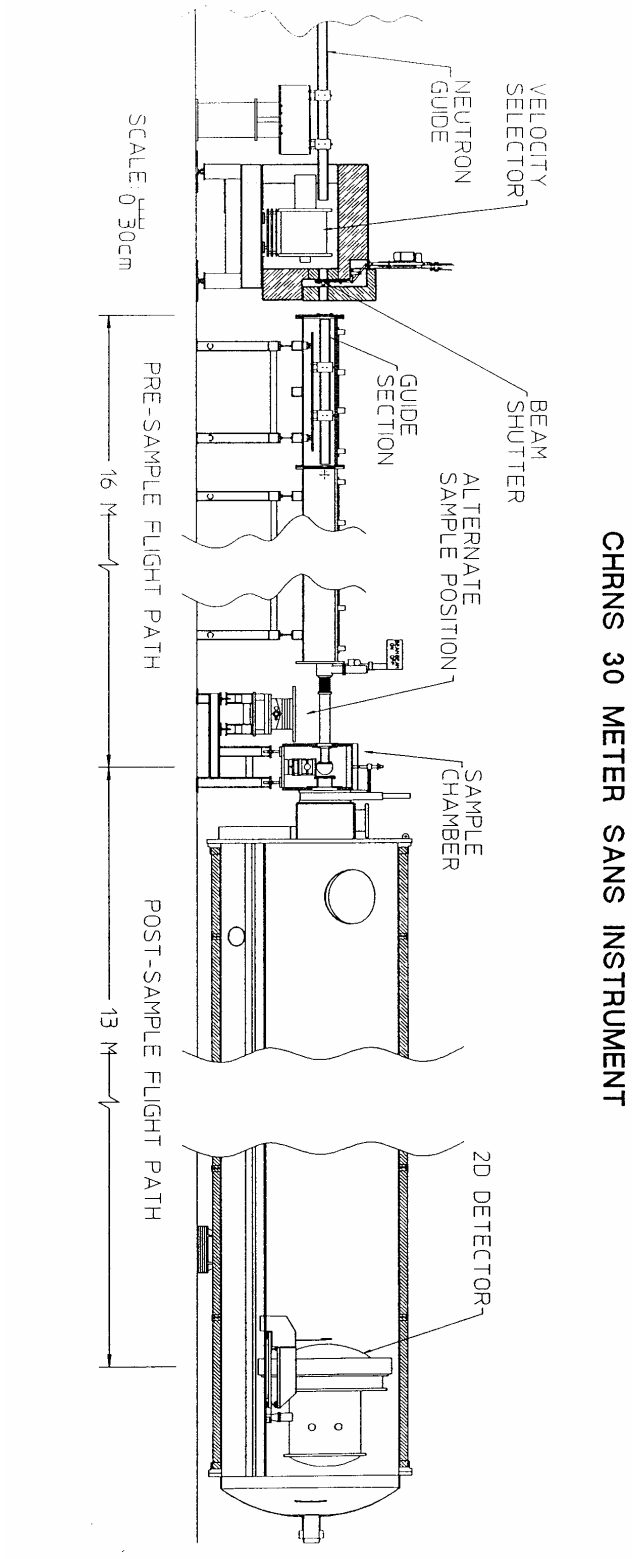

Figure V. 1: Schematics of a 30m SANS instrument at NIST.

Table V. 1: 30 m NIST-SANS Instruments Characteristics.

Source:	neutron guide (NG3), 6 x 6 cm^2		
	neutron guide (NG7), 5 x 5 cm^2		
Monochromator:	mechanical velocity selector with variable speed and pitch		
Wavelength Range:	variable from 0.5 to 2.0nm		
Wavelength Resol.:	10 to 30% for $\Delta\lambda/\lambda$ (FWHM)		
Source-to-Sample Distance:	3.5 to 15m in 1.5m steps via insertion of neutron guide segments		
Sample-to-Det. Dist.:	1.3 to 13.2m continuously variable for NG3 1.3 to 15.3m continuously variable for NG7		
Collimation:	circular pinhole collimation		
Sample Size:	0.5 to 2.5cm diameter		
Q-range:	0.01 to 6nm^{-1}		
Size Regime:	1 to 600nm		
Detector:	64 x 64 cm^2 He-3 position-sensitive proportional counter (1 cm^2 resolution), ILL type		
Ancillary Equipment:	-automatic multi-specimen sample changer with temperature control from -10 to 200 ^oC -electromagnet (0 to 9Tesla) -Couette flow shearing cell -cryostats and vacuum furnace (10 to 1800 K) -pressure cell (0 to 1x10^8 Pa, 25^oC to 160^oC)		
Neutrons on Sample vs. Q_{min}	Q_{min} (nm^{-1})	I_s[a] (n/sec)	I_s[b] (n/sec)
	0.015	3x10^3	2x10^4
	0.02	2x10^4	9x10^4
	0.04	2x10^5	9x10^5
	0.10	1x10^6	5x10^6

[a] for 1.5 cm diameter sample, $\Delta\lambda/\lambda$=0.25, 15 MW reactor power and D_2O-ice cold source

[b] for 1.5 cm diameter sample, $\Delta\lambda/\lambda$=0.15, 20 MW reactor power and liquid hydrogen cold source

V. 2 . Time of Flight SANS Instrument Components

A time of flight SANS instrument comprises some of the main features described above (collimation, sample chamber, flight paths, area detector, etc) as well as some other features described here:

-- A source chopper to define the starting neutron pulse.

-- The area detector is synchronized to the source chopper so that a number of wavelength frames (for example 128) are recorded for each pulse. No monochromator is necessary with the time of flight method.

-- A supermirror bender can be used (as on the LOQ instrument at ISIS for example) to remove short wavelengths and let the instrument get out of the direct line of sight from the source. Note

that curved guides have a cutoff wavelength below which neutrons are not transmitted. This bender replaces the filter.

-- High wavelengths (say above 14A) have to be eliminated in order to avoid frame overlap. This can be done by gating the detector or through the use of frame overlap mirrors (as on the LOQ instrument at ISIS). Reflecting mirrors are set at a slight angle (1^{o}) from the beam direction so as to reflect only long wavelength neutrons (note that the reflection critical angle varies linearly with wavelength).

Because of the wide wavelength range used in time of flight instruments, materials that display a Bragg cutoff (such as sapphire windows) cannot be used. Data reduction becomes more complex with time of flight instruments because most corrections (transmission, monitor normalization, detector efficiency, linearity, uniformity, etc) become wavelength dependent. Time of flight instruments have the advantage, on the other hand, of measuring a wide Q range at once. Also the large number of wavelength frames can be kept separate therefore yielding very high wavelength resolution ($\Delta\lambda/\lambda<1\%$) which is useful for highly ordered samples (some fibers are crystalline in one direction with essentially "perfect" mosaic spread).

V. 2. Sample Environments

Typical sample thickness for SANS measurements is of order of 1 mm. Liquid samples (polymer solutions, microemulsions) are often contained in quartz cells into which syringes can be inserted. Solid polymer samples are usually melt pressed above their softening (glass-rubber) temperature, then confined in special cells between quartz windows.

Flexibility of design for some instruments allows the use of typical size samples under temperature control or bulky sample environments. Temperature is easily varied between ambient temperature and 200^{o}C using heating cartridges or between -10^{o}C and room temperature using a circulating bath. Other sample environment equipment such as low-temperature cryostats (4 to 350 K) and electromagnets (1-10Teslas) are sometime made available to users. Various shear cells (Couette, plate-and-plate, etc) are helping probe "soft" materials at the molecular level in order to better understand their rheology. A few pressure cells are also finding wide use for investigations of compressibility effects on the thermodynamics of phase separation as well as on structure and morphology.

V. 3. SANS Measurements

SANS measurements using cold neutrons take from a few minutes to an hour when measuring typical polymer samples. The process starts by sample preparation, which consists in weighing the right amounts of polymers and solvents and mixing them to form homogeneous mixtures. If polymer blends are the desired outcome, solvent is evaporated, sample is dried then hot pressed to yield the right size and thickness sample.

A reasonable instrument configuration is chosen at first by setting a low wavelength and varying the sample-to-detector distance so as to optimize the desired Q-range. If the maximum available sample-to-detector distance is reached, wavelength is then increased. Choice of the source-to-sample distance, wavelength spread, and aperture sizes are dictated by the desired instrumental resolution (sharp scattering features require good resolution) and flux on sample. Scattered intensity is proportional to many factors that have to be optimized: $I(Q)=\phi ATd[d\Sigma/d\Omega]\Delta\Omega\varepsilon t$ (ϕ: flux, A: sample area, T: transmission, d: sample thickness, ε: detector efficiency, t: counting time).

Transmission measurements are usually performed at the beginning of an experiment. In order to avoid complicated multiple scattering corrections, sample transmissions are kept high (>60%).

A complete set of data involves measurements from the sample, from an incoherent (usually nondeuterated) scatterer that yields flat signal, from the empty cell and a blocked beam and from a calibrated (absolute standard) sample. SANS data are corrected, rescaled to give a macroscopic cross section (units of cm^{-1}) then averaged (circularly for isotropic scattering or sector-wise for anisotropic scattering). Reduced data are finally plotted using standard linear plots (Guinier, Zimm, Kratky, etc) in order to extract qualitative trends for sample characteristics (radius of gyration, correlation length, persistence length, etc) or fitted to models for more detailed data analysis.

References:

K. Ibel, "The SANS Camera D11 at the High Flux Reactor, Grenoble", J. Appl. Cryst. 9, 296 (1976).

D.F.R. Mildner, R. Berliner, O.A. Pringle, J.S. King, "The SANS Spectrometer at the University of Missouri Research Reactor", J. Appl. Cryst. 14, 370 (1981).

C.J. Glinka, J.M. Rowe, J.G. LaRock, "The SANS Spectrometer at NBS", J. Appl. Cryst. 19, 427 (1986). Note that NIST used to be called NBS.

Y. Ishikawa, M. Furusaka, N. Niimura, M. Arai, K. Hasegawa, "The TOF SANS Spectrometer at the KENS Pulsed Cold Source", J. Appl. Cryst. 19, 229 (1986).

W.C. Koehler, "The National Facility for SANS", Physica (Utrecht) 137B, 320 (1986).

P. Seeger, R.P. Hjelm, "The Low-Q Diffractometer at the LANSC", Molecular Cystrals, Liquid Crystals 180A, 101 (1990).

V. 4. Questions

1. Why are small-angle neutron scattering instruments bigger than small-angle x-ray scattering instruments?
2. Why aren't crystal monochromators used instead of velocity selectors in SANS instruments?
3. Could one perform SANS measurements without using an area detector?
4. What is the useful range of cold neutron wavelengths?
5. When is it necessary to use wide wavelength spread $\Delta\lambda/\lambda$?
6. Find out how does a velocity selector work?
7. How does a He-3 area detector work?
8. What is the cost of building a SANS instrument?
9. Name some materials used for neutron windows.
10. Do cold neutrons destroy samples?

VI. THE NEUTRON SCATTERING TECHNIQUE

VI. 1. Various Radiation Used for Scattering

Many forms of radiation can be used for scattering purposes: X-rays, neutrons, electrons, laser light, gamma rays, etc. These have different characteristics and are used for different purposes. Table VI.1 summarizes various scattering methods.

Table VI. 1: Various radiations used in scattering

Type of Radiation	X-Rays	Neutrons	Electrons	Laser Light
Wavelength Range:	0.1-5A:X-rays 5A-1μm:VUV	1 A-15 A	0.1 A	1 μm
Sensitive to inhomogeneities:	Electron Density	Density of Nuclei	Electron Cloud	Polarizabil. (Refractive Index)
Scatt. Methods	SAXS,WAXS	SANS,WANS	LEED	SLS
Samples Thickness:	< 1 mm	1-2 mm	100 μm	1-5 mm
Problems with:	Absorption	Low Fluxes	Low Penetration	Dust Scatt.

The small-angle neutron and X-ray scattering methods (SANS, SAXS) are useful for polymer research because they probe size scales from the near atomic to the near micron. Static light scattering (SLS) complements these techniques by focussing on the micron length scale. Other methods such as wide-angle neutron and X-ray scattering (WANS, WAXS) and low-energy electron diffraction (LEED) probe very local (atomic) structures.

Neutron scattering is the technique of choice for condensed matter investigations in general because thermal/cold neutrons do not deposit energy in the scattering specimen. For instance, neutrons of 1 A wavelength have much lower kinetic energy (82meV) than x-rays and electrons of the same wavelength (12keV and 150eV respectively).

VI. 2. Characteristics of Neutron Scattering

A few advantages of neutron scattering follow:

-- Neutron scattering lengths vary "randomly" with atomic number and are independent of momentum transfer Q. This is used to advantage in deuterium labeling using the fact that the scattering lengths of hydrogen and deuterium are widely different (-0.3741 and 0.6674 $x10^{-12}$ cm respectively). The negative sign in front of b_H means that the phase of the wavefunction is inverted during scattering.

-- Neutrons have high penetration (low absorption) for most elements making neutron scattering a bulk probe. Sample environments can be designed with high Z materials (aluminum, quartz, sapphire, etc).

-- Neutrons have the right momentum transfer and right energy transfer for investigation of both structures and dynamics in condensed matter. The neutron-spin-echo method has found wide use in polymer dynamics studies; this method falls outside of our scope.

-- A wide range of wavelengths can be achieved by the use of cold sources. One can reach very low Q's and overlap with static light scattering (SLS) using a double crystal monochromator (so called Bonse Hart) instrument.

-- Since neutron detection is through nuclear reactions (rather than direct ionization for example) the detection signal-to-noise ratio is high (MeV energies released as kinetic energy of reaction products).

A few disadvantages of neutron scattering follow:

-- Neutron sources are very expensive to build and to maintain. It costs millions of dollars annually to operate a nuclear research reactor and it costs that much in electrical bills alone to run a pulsed neutron source. High cost (billions of US$) was a major factor in the cancellation of the Advanced Neutron Source project.

-- Neutron sources are characterized by relatively low fluxes compared to X-ray sources (synchrotrons) and have limited use in investigations of rapid time dependent processes.

-- Relatively large amounts of samples are needed: 1 mm-thickness and 1 cm diameter samples are needed for SANS measurements. This is a difficulty when using expensive deuterated samples or precious (hard to make) biology specimens.

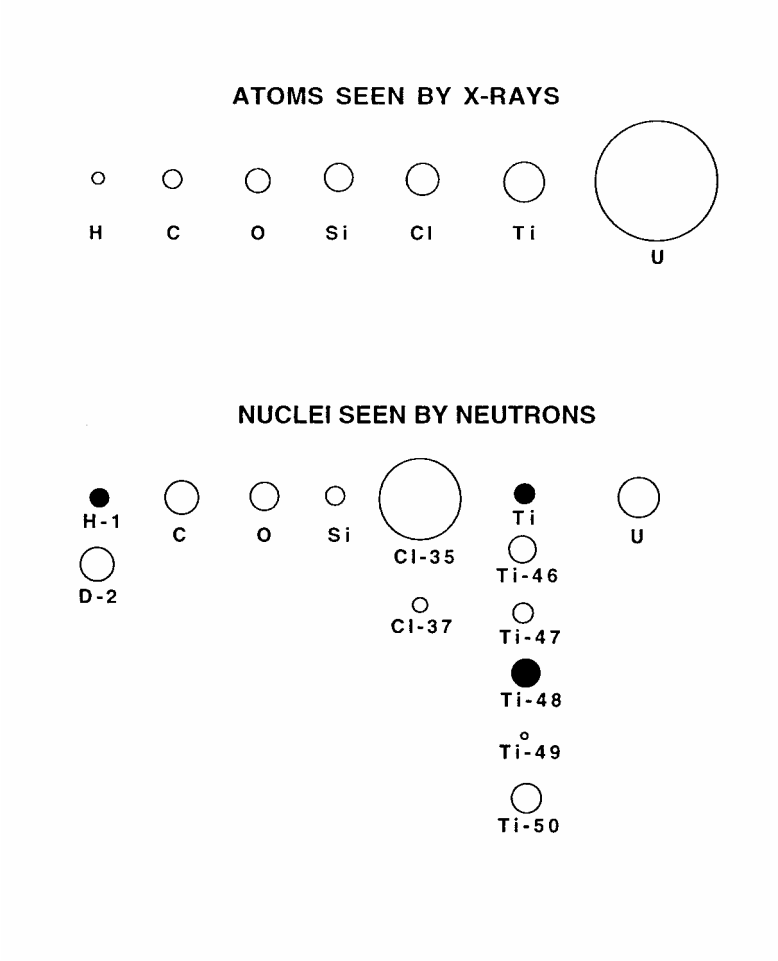

Figure VI. 1: Neutrons are scattered from nuclei while X-rays are scattered from electrons. Scattering lengths for a few elements relevant to polymers are compared. Ti and U have also been included. Negative neutron scattering lengths are represented by dark circles.

Reference

D.L Price and K. Skold, "Introduction to Neutron Scattering" Methods of Experimental Physics 23A, 1 (1986)

"NIST Cold Neutron Research Facility", National Institute of Standards and Technology Journal of Research, 98, Issue No 1 (1993).

VII. NEUTRON SCATTERING LENGTHS AND CROSS SECTIONS

Scattered intensity is proportional to the so called "contrast factor" which contains the scattering lengths. This and other terminology is introduced here along with elements of scattering theory.

VII.1. Scattering Lengths

Consider a plane wave (well collimated neutron beam) incident on a nucleus. The scattered wave is spherical and the wavefunction (at large distances) is of the form:

$$\exp(i\mathbf{k_i}.\mathbf{r}) + f(\theta)\exp(ik_S|r-r'|)/|r-r'| \qquad \text{(Eq. VII.1)}$$

where $f(\theta)$ is the scattering amplitude. The scattering vector $\mathbf{Q}=\mathbf{k}_i-\mathbf{k}_S$ characterizes the probed length scale and its magnitude is given for elastic scattering in terms of the neutron wavelength λ and scattering angle θ as $Q=4\pi\sin(\theta/2)/\lambda$. For small angles (SANS), it is simply approximated by $Q=2\pi\theta/\lambda$. Because Q is the Fourier variable (in reciprocal space) conjugate to scatterer positions (in direct space), investigating low-Q probes large length scales in direct space.

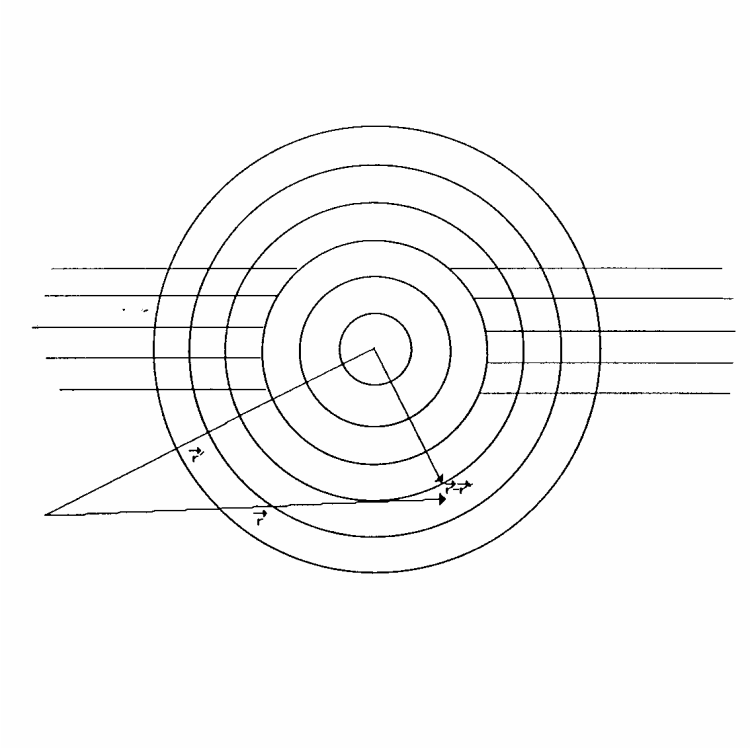

Figure VII.1: Incident and scattered waves.

An orbital angular momentum characterizes each neutron incident on the scattering nucleus. For thermal/cold neutrons, only "s wave" scattering (corresponding to a zero orbital angular quantum number) is important, "p wave" scattering becomes important only above neutron energies of 200 keV, which has no contribution in scattering applications. In this case (s-wave scattering) a phase shift δ_0, and a scattering length a can be defined (Sears, 1992):

$$f(\theta) = (1/2iQ)\,[\exp(i\delta_0) - 1] \cong -a + iQ\,a^2 + \ldots \qquad \text{(Eq. VII.2)}$$

where Q is the neutron wavenumber. The scattering length itself can be complex if absorption is non negligible: $a = a_R - ia_I$, although neutron absorption is small for typical polymer samples.

Moreover, since no nucleus is completely free, bound scattering lengths should be used instead: $b = a\,(A + 1)/A$, where A is the atomic number. Free and bound scattering lengths are substantially different only for low mass elements such as hydrogen.

The differential scattering cross section $d\sigma/d\Omega$ depends on two quantities: (1) a technique-dependent factor which for neutron scattering is called the contrast factor and (2) a sample-dependent term which is called the static structure factor and represents the structure of the scattering environment in the sample.

VII. 2. Scattering Cross Sections

The microscopic differential scattering cross section is given by: $d\sigma(\theta)/d\Omega = |f(\theta)|^2$. It is also defined more practically as:

$$d\sigma(\theta)/d\Omega = \frac{\text{number of scattered neutrons inside a solid angle } d\Omega \text{ with scattering angle } \theta \text{ per nucleus per sec}}{\text{number of incident neutrons per cm}^2 \text{ per sec}}$$

This cross section contains information about what inhomogeneities are scattering and how they are distributed in the sample (chain conformations, morphology, etc). The microscopic scattering cross section is its integral over solid angles: $\sigma_S = \int [d\sigma_S/d\Omega]\, d\Omega$ and is given by: $\sigma_S = 4\pi|b|^2$ (units of barn=10^{-24} cm^2). Bound scattering lengths b and cross sections σ_S are tabulated (Sears, 1992; Koester et al, 1991).

Given the number density N (number of scattering nuclei/cm^3) in a material, a macroscopic cross section is also defined as: $\Sigma = N\sigma$ (units of cm^{-1}). SANS data are often presented on an "absolute" macroscopic cross section scale independent on instrumental conditions and on sample volume; this is: $d\Sigma/d\Omega = Nd\sigma/d\Omega$.

VII. 3. Estimation of Neutron Scattering Lengths

A simple argument is used here in order to appreciate the origin of the scattering length. Consider a neutron of thermal/cold incident energy E_i being scattered from a nucleus displaying an attractive square well $-V_o$ (simplest model) potential (Note that $V_o >> E_i$). The Schroedinger equation:

$$[-(h^2/8\pi^2 m)\nabla^2 + V(r)]\, \psi = E\, \psi \qquad \text{(Eq. VII.3)}$$

can be solved in 2 regions (inside and outside of the well region).

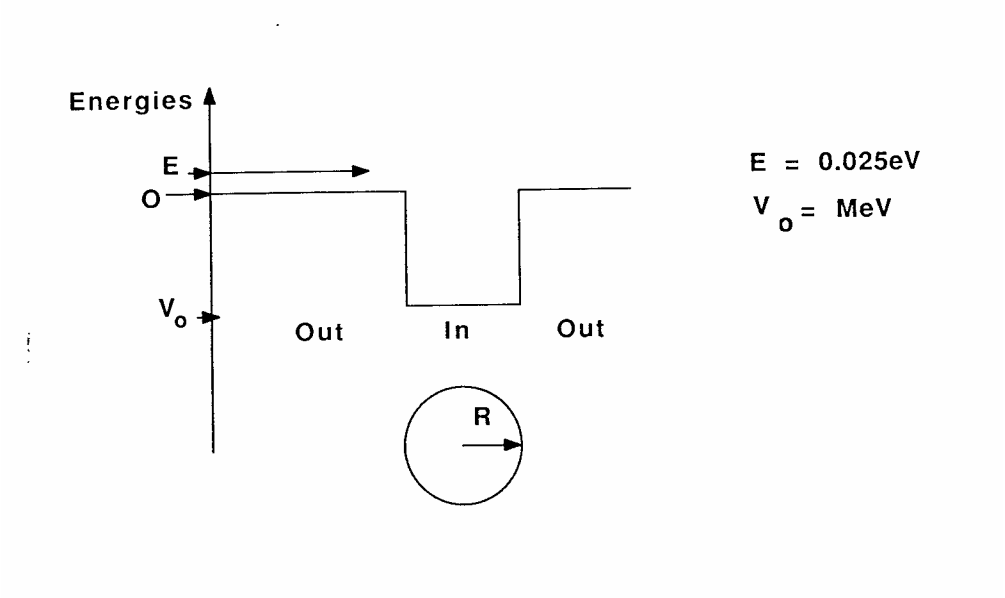

Figure VII. 2: Neutron scattering from the quantum well of a nucleus.

Outside of the well region (i.e., for r>R) where V(r) = 0, the solution has the form:

$$\psi_S^{Out} = [\sin(kr)/kr] - [b \exp(ikr)/r] \quad \text{(s-wave scattering)} \qquad \text{(Eq. VII.4a)}$$

and $k=[2mE_i]^{1/2}2\pi/h$; whereas inside of the well (R >r>-R) where V(r) = $-V_0$ the solution is of the form:

$$\psi_S^{In} = A\,[\sin(qr)/qr] \quad \text{with } q=[2m(E_i+V_0)]^{1/2}2\pi/h. \qquad \text{(Eq. VII.4b)}$$

The continuity boundary conditions are applied at the surface (r=R):

$$\psi_S^{In}(r=R) = \psi_S^{Out}(r=R) \qquad \text{(Eq. VII.5a)}$$

$$d[r\psi_S^{In}(r=R)]/dr = d[r\psi_S^{Out}(r=R)]/dr \qquad \text{(Eq. VII.5b)}$$

with $kR = (2mE_i)^{1/2}R2\pi/h << 1$ and therefore $\psi_S^{Out} \sim 1 - b/r$. Thus:

$$\begin{cases} A\sin(qR)/q = R-b \\ A\cos(qR) = 1 \end{cases} \Rightarrow \begin{cases} A = 1/\cos(qR) & \text{(Eq. VII.6a)} \\ b/R = 1-\tan(qR)/qR. & \text{(Eq. VII.6b)} \end{cases}$$

The solution of this equation:

$$b/R = 1 - \tan(qR)/qR \qquad \text{(Eq. VII.7)}$$

gives a first order estimate of the scattering length b if the radius of the spherical nucleus R and the depth of the potential well V_0 are known.

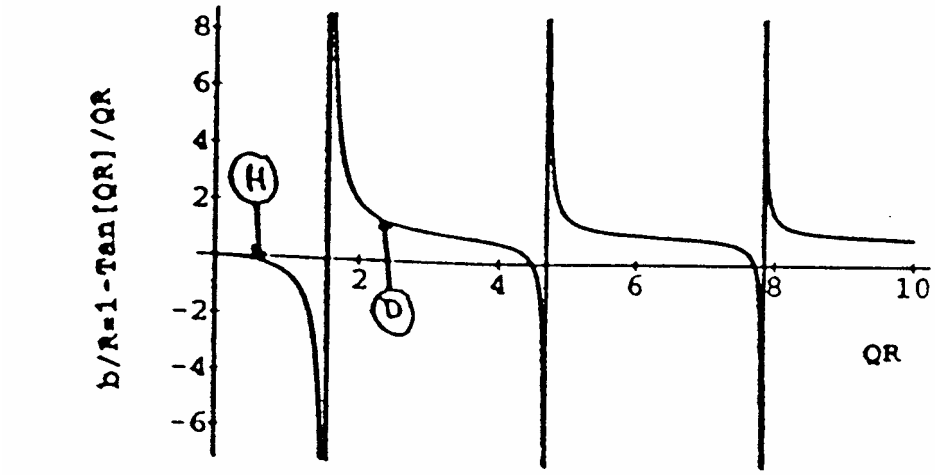

Figure VII. 3: Solution of the Schroedinger equation subject to the boundary conditions.

Because of the steep variation of the solution to the above equation, adding only one nucleon (for example, going from H to D) gives a very large (seemingly random) variation in b. The scattering

length can be negative (case where the wavelength has a phase change of 180^o during scattering) like for H-1, Li-7, Ti-48, Ni-62, etc. Note that absorption has been neglected in this simple model since it is negligible for polymer systems.

Table VII.1: Coherent and incoherent neutron scattering lengths (b_c and b_i) and cross sections (σ_c and σ_i) as well as absorption cross section (σ_a) for atoms commonly found in polymers.

Element	b_c fermi	b_i fermi	σ_c barn	σ_i barn	σ_a barn
H-1	-3.739	25.274	1.757	80.26	0.333
D-2	6.671	4.04	5.592	2.05	0.000
C-14	6.646	0	5.550	0.001	0.003
N-14	9.36	2.0	11.01	0.50	1.90
0-16	5.803	0	4.232	0.000	0.000
F-19	5.654	0	4.232	0.001	0.000
Na-23	3.63	3.59	1.66	1.62	0.530
Si-28	4.149	0	2.163	0.004	0.171
P-31	5.13	0.2	3.307	0.005	0.172
S-32	2.847	0	1.017	0.007	0.53
Cl-35	9.577	0.65	11.526	5.3	33.5

1 fermi=10^{-13} cm
1 barn=$10^{-24}cm^2$

References:

V.F. Sears, "Neutron Scattering Lengths and Cross Sections", Neutron News 3, 26, (1992)

L. Koester, H. Rauch, and E. Seymann, "Neutron Scattering Lengths: a Survey of Experimental Data and Methods", Atomic Data and Nuclear Data Tables 49, 65 (1991)

VIII. COHERENT/INCOHERENT NEUTRON SCATTERING

Neutron scattering is characterized by coherent and incoherent contributions at the same time. Whereas coherent scattering depends on Q and is therefore the part that contains information about scattering structures, incoherent scattering does not.

VIII. 1. Separate the Coherent and Incoherent Parts

Here, the coherent and incoherent parts of the elastic scattering cross section are separated. Consider a set of N nuclei with scattering lengths b_i in the sample. The scattering cross section is given by:

$$d\sigma(\theta)/d\Omega = |f(\theta)|^2 = (2\pi m/h^2)^2 \; |\int d\mathbf{r} \exp(-i\mathbf{Q}.\mathbf{r}) \; V(r)|^2 \qquad \text{(Eq. VIII.1)}$$

where $\mathbf{Q} = \mathbf{k}_i - \mathbf{k}_S$ and V(r) is the Fermi pseudopotential describing neutron-nuclear interactions:

$$V(r) = (h^2/2\pi m) \sum_{i=1}^{N} b_i \, \delta(r - r_i); \qquad \text{(Eq. VIII.2)}$$

where $\mathbf{r}_i$ is the position and b_i the scattering length of nucleus i. Therefore, the differential scattering cross section is the sum of the various scattering phases from all of the nuclei in the sample properly weighed by their scattering lengths:

$$d\sigma(\theta)/d\Omega = \sum_{i=1}^{N} \sum_{j=1}^{N} b_i b_j \langle \exp[i\mathbf{Q}.(\mathbf{r}_i - \mathbf{r}_j)] \rangle \qquad \text{(Eq. VIII.3)}$$

where <...> represents an ensemble average (average over scatterers positions).

Consider an average over a "blob" consisting of a number m of nuclei in the sample:

$$\{...\} = (1/m) \sum_{i=1}^{m} ... \qquad \text{(Eq. VIII.4)}$$

This average could be over 1 cm^3 of material for multicomponent atomic samples, it could be over one monomeric unit for macromolecular systems or over all atoms in one molecule for single component molecular systems.

Define average and fluctuating parts: $b_i = \{b\} + \delta b_i$ and $\mathbf{r}_i = \mathbf{R}_\alpha + \mathbf{S}_{ai}$ as well as:

$\mathbf{R}_\alpha$: position of the center of mass of blob α

$\mathbf{S}_{\alpha i}$: relative position of scatterer i inside blob α

m: number of nuclei per blob (think "per monomer")

M: number of blobs (think "monomers") in the sample (Note that N = mM).

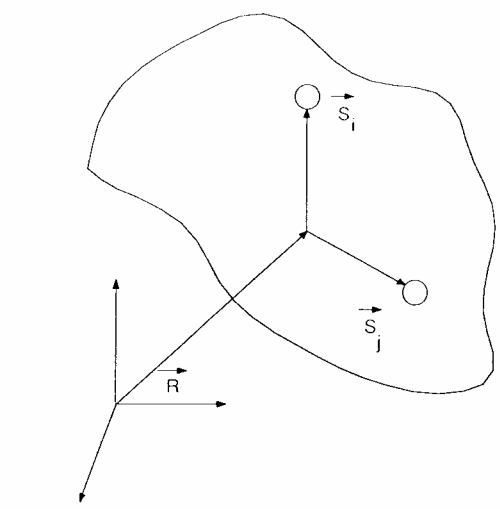

Figure VIII. 1: Parametrization of a scattering molecule.

The various terms of the scattering cross section can be separated as:

$$d\sigma(\theta)/d\Omega = \sum_{ij}^{N} [\{b\} + \delta b_i][\{b\} + \delta b_j]\langle \exp(i\mathbf{Q}.(\mathbf{r}_i-\mathbf{r}_j))\rangle \qquad \text{(Eq. VIII.5)}$$

$$= \{b\}^2 \sum_{ij}^{N} \langle \exp(i\mathbf{Q}.\mathbf{r}_{ij})\rangle + \sum_{ij}^{N} \delta b_i \delta b_j \langle \exp(i\mathbf{Q}.\mathbf{r}_{ij})\rangle + 2\{b\} \sum_{ij}^{N} \delta b_i \langle \exp(i\mathbf{Q}.\mathbf{r}_{ij})\rangle$$

where $\mathbf{r}_{ij} = \mathbf{r}_i - \mathbf{r}_j$. If $\mathbf{r}_{ij}$ is approximated by $\mathbf{R}_{\alpha\beta}$ which is equivalent to $S_{\alpha i} << R_\alpha$ (all nuclei of one blob are located very close to each other) the term:

$$\sum_{i}^{N} \delta b_i \langle \exp(i\mathbf{Q}.\mathbf{r}_{ij})\rangle \cong [\sum_{i}^{N} \delta b_i] \langle \exp(i\mathbf{Q}.\mathbf{R}_{\alpha\beta})\rangle = 0 \qquad \text{(Eq. VIII.6)}$$

can be neglected (because $\{\delta b_i\}=0$ by definition) and the term:

$$\sum_{ij}^{N} \delta b_i \delta b_j \langle \exp(i\mathbf{Q}.\mathbf{r}_{ij})\rangle$$

contributes only when i=j. In that case, the scattering cross section can be written simply as the sum of two contributions:

$$d\sigma(\theta)/d\Omega = \{b\}^2 \sum_{ij}^{N} \langle \exp(i\mathbf{Q}.\mathbf{r}_{ij})\rangle + \sum_{ij}^{N} \delta b_i^2 \qquad \text{(Eq. VIII.7)}$$

$$= (d\sigma(\theta)/d\Omega)_{coh} + (d\sigma/d\Omega)_{incoh}.$$

The last term is the incoherent cross section for the whole sample:

$$(d\sigma/d\Omega)_{incoh} = N\{\delta b^2\} = N\{b^2\} - N\{b\}^2. \qquad \text{(Eq. VIII.8)}$$

Usually incoherent scattering cross sections are defined for each monomer instead as $m\{\delta b^2\}$ where m is the number of atoms per monomer.

VIII. 2. Isotopic Incoherence

Even homonuclear systems have different components (different isotopes) mixed according to their natural abundances. Scattering length tables contain values for the isotopes as well as their natural mixtures. For a mixture, the following average should be performed:

$$\{b\} = \sum_{i}^{N} A_i\, b_i \qquad \text{(Eq. VIII.9)}$$

where b_i is the scattering length of isotope i and A_i is its abundance (in weight %). Note that in multiple component systems, an averaging is to be performed also over all components. The incoherent cross section involves the average deviation from the square: $\{\delta b^2\} = \{b^2\} - \{b\}^2$

where: $\{b^2\} = \sum_{i}^{N} A_i\, b_i^2$.

VIII. 3. Spin Incoherence

Nuclei with nonzero spins contribute to spin incoherence since they yield a specific number of neutron-nucleus spin states during the scattering process. The neutron spin of 1/2 couples to the nuclear spin I to give:

-- 2I+2 states (noted b_+) corresponding to parallel spins
-- 2I states (noted b_-) corresponding to antiparallel spins

so that there is a total of 2(2I+1) states with weighing factors

$$W_+ = (2I+2)/2(2I+1) \text{ and } W_- = 2I/2(2I+1). \qquad \text{(Eq. VIII.10)}$$

The averages over spin states are calculated as

$$\{b\} = W_+b_+ + W_-b_- = [(I+1)b_+ + Ib_-]/(2I+1) \qquad \text{(Eq. VIII.11)}$$
$$\{b^2\} = W_+b_+^2 + W_-b_-^2 = [(I+1)b_+^2 + Ib_-^2]/(2I+1)$$

using tabulated values of either b_+ and b_- or:

$$b_{coh} = W_+b_+ + W_-b_- \qquad \text{(Eq. VIII.12)}$$
$$b_{incoh} = (W_+W_-)^{1/2}(b_+ - b_-)$$

(most tables contain b_{coh} and b_{incoh} instead of b_+ and b_-). The spin-dependent scattering length can therefore be written as:

$$b = b_{coh} + 2b_{incoh}\mathbf{s.I}/[I(I+1)]^{1/2} \qquad \text{(Eq. VIII.13)}$$

The coherent part is separated from the incoherent one experimentally using deuterium labeling.

VIII. 5. Coherent Scattering Lengths for a Few Monomers and a Few Solvents

The following two tables summarize scattering lengths for a few monomers and a few commonly used solvents. These have been calculated using tabulated values for the scattering lengths of the various elements and their relative amounts.

Table VIII.1: Coherent Scattering Lengths for a Few Synthetic Monomers (in units of 10^{-12} cm)

Polymer Name	Formula	Hydrogenated	Deuterated
Polystyrene	$[CH_2\text{-}CH(C_6H_5)]$	2.330	10.662
Polymethylmethacrylate	$[CH_2\text{-}C(CH_3)(CO_2CH_3)]$	1.495	9.827
Polymethylacrylate	$[CH_2\text{-}CH(CO_2CH_3)]$	1.578	7.827
Polyvinylchloride	$[CH_2CH(Cl)]$	1.378	4.503
Polyethylene	$[CH_2\text{-}CH_2]$	-0.166	4.00
Polycarbonate	$[C_6H_4\text{-}C(CH_3)_2C_6H_4\text{-}O\text{-}CO_2]$	7.150	21.730
Polyvinylmethylether	$[CH_2OH(OCH_3)]$	0.332	6.581
Polytetrahydrofuran	$[C_4OH_6]$	0.997	7.246
Poly α Chlorostyrene	$[CH_2\text{-}CH(C_6H_4Cl)]$	3.874	11.164
Polyurethane (Ethylcarbonate)	$[NH\text{-}CO_2\text{-}CH_2\text{-}CH_2]$	2.223	7.431

Table VIII. 2: Coherent Scattering Lengths for some Solvents (in units of 10^{-12} cm)

Solvent Name	Formula	Hydrogenated	Deuterated
Toluene	$C_6H_5CH_3$	1.664	9.996
Benzene	C_6H_6	1.747	7.996
Cyclohexane	C_6H_{12}	-0.497	12.001
Acetone	$CH_3\text{-}COCH_3$	0.332	6.5821
Chloroform	$CHCl_3$	3.160	4.205
Methylene Chloride	CH_2Cl_2	2.257	4.340
Carbon Disulfide	CS_2	1.226	
Tetrahydrofurane	C_4OH_8	0.247	8.581
Tri-m-Tolylphosphate	$CH_3\text{-}C_6H_2P_3$	4.326	9.553
Trimethylbenzene	$C_6H_3(CH_3)_3$	1.498	13.996

VIII. 6. A Few Neutron Contrast Factors for Polymer Mixtures

Consider a two-component polymer system (say polymer1 homogeneously mixed in polymer 2). The neutron contrast is defined as the square of the difference between two scattering length densities $(b_1/V_1 - b_2/V_2)^2$ where b_1 and b_2 are the scattering lengths for monomers 1 and 2 and V_1 and V_2 are the monomer molar volumes for the two components. Component 2 could represent a solvent for polymer solutions. A few contrast factors have been calculated for the following polymer mixtures.

Deuterated Polystyrene/Polyvinylmethyether (dPS/PVME) Blend:

PSD: C_8D_8, $b_{PSD}=1.06\times10^{-11}$ cm, $V_{PSD}=100$ cm^3/mole

PVME: C_3H_6O, $b_{PVME}=3.30\times10^{-13}$ cm, $V_{PVME}=55.4$ cm^3/mole

$(b_{PSD}/V_{PSD} - b_{PVME}/V_{PVME})^2N_{av} = 6.03\times10^{-3}$ mole/cm^4 , N_{av}: Avogadro's No

Deuterated Polystyrene/Hydrogenated Polystyrene (dPS/hPS) Blend:

PSD: C_8D_8, $b_{PSD}=1.06\times10^{-11}$ cm, $V_{PSD}=100$ cm^3/mole

PSH: C_8H_8, $b_{PSH}=0.23\times10^{-11}$ cm, $V_{PSH}=100$ cm^3/mole

$(b_{PSD}/V_{PSD} - b_{PSH}/V_{PSH})^2N_{av} = 4.15\times10^{-3}$ mole/cm^4

Deuterated Polystyrene/Polybutylmethacrylate (dPS/PBMA) Blend:

PSD: C_8D_8, $b_{PSD}=1.06\times10^{-11}$ cm, $V_{PSD}=100$ cm^3/mole

PBMA: $C_8H_{14}O_2$, $b_{PBMA}=1.24\times10^{-12}$ cm, $V_{PBMA}=133$ cm^3/mol

$(b_{PSD}/V_{PSD} - b_{PBMA}/V_{PBMA})^2N_{av} = 5.61\times10^{-3}$ mole/cm^4

Polystyrene/Polyisoprene (PS/PI) Blend:

PSH: C_8H_8, $b_{PSH}=0.23\times10^{-11}$ cm, $V_{PSH}=100$ cm^3/mole

PSD: C_8D_8, $b_{PSD}=1.06\times10^{-11}$ cm, $V_{PSD}=100$ cm^3/mole

PIH: C_5H_8, $b_{PIH}=0.33\times10^{-12}$ cm, $V_{PIH}=76$ cm^3/mole

$(b_{PSH}/V_{PSH} - b_{PIH}/V_{PIH})^2N_{av} = 2.09\times10^{-4}$ mole/cm^4

$(b_{PSD}/V_{PSD} - b_{PIH}/V_{PIH})^2N_{av} = 6.20\times10^{-3}$ mole/cm^4

Deuterated Polystyrene/Dioctylphthalate (dPS/DOP) Solution:

PSD: C_8D_8, $b_{PSD}=1.06\times10^{-11}$ cm, $V_{PSD}=100$ cm^3/mole

DOP: $C_{24}H_{38}O_4$, $b_{DOP}=4.07\times10^{-12}$ cm, $V_{DOP}=390$ cm^3/mole

$(b_{PSD}/V_{PSD} - b_{DOP}/V_{DOP})^2N_{av} = 5.48\times10^{-3}$ mole/cm^4

References

W. Marshall and S.W. Lovesey, "Theory of Thermal Neutron Scattering", Clarendon Press, Oxford (1971).

G.E. Bacon, "Neutron Diffraction", Clarendon Press, Oxford (1975).

VIII. 7. Questions

1. Whereas x-rays are scattered by the atomic electron cloud, neutrons are scattered by what part of the atom?
2. Are higher fluxes achieved in research reactors (neutron sources) or in synchrotron x-ray sources?
3. Is partial deuteration always needed for neutron scattering from polymers?
4. What is the origin of the name for neutron cross sections (barn)?
5. Why aren't x-rays characterized by spin-incoherence as neutrons do?

6. Work out the relative composition of an H_2O/D_2O mixture that would have zero average coherent cross section (so called semi-transparent mixture).
7. Comparing the coherent scattering cross sections for a deuterated polymer in hydrogenated solvent and a hydrogenated polymer in deuterated solvent, which one has the highest signal-to-noise ratio?
8. Why does carbon have a negligible incoherent scattering cross section?
9. What is the meaning of a negative scattering length?
10. Work out the scattering contrast for a polymer mixture of your choice (research interest).

IX. SINGLE-PARTICLE STRUCTURE FACTORS

IX. 1. Definitions

Consider a sample consisting of N scatterers (think monomers) of coherent scattering length {b} each occupying a sample volume V. The scatterer density (and its Fourier transform) are defined as:

$$n(r) = \sum_{i}^{N} \delta(\mathbf{r}-\mathbf{r}_i) \text{ and } n(Q) = \sum_{i}^{N} \exp[i\mathbf{Q}.\mathbf{r}_i]. \qquad \text{(Eq. IX.1)}$$

Note that these quantities vary randomly with position **r** and momentum **Q**. The average density being constant (<n(r)>=n=N/V), a fluctuating density (and its Fourier transform) are:

$$\Delta n(r) = \sum_{i}^{N} \delta(\mathbf{r}-\mathbf{r}_i) - n \text{ and } \Delta n(Q) = \sum_{i}^{N} \exp[i\mathbf{Q}.\mathbf{r}_i] - (2\pi)^3 n\delta(\mathbf{Q}) \quad \text{(Eq. IX.2)}$$

where $\delta(\mathbf{Q})$ is the Dirac delta function which does not contribute except at **Q=0** (along the very forward direction) which is experimentally irrelevant. The static structure factor for the system is defined as the density-density correlation function:

$$S(Q) = \langle n(-Q)n(Q)\rangle = \sum_{ij}^{N} \langle \exp[i\mathbf{Q}.(\mathbf{r}_i-\mathbf{r}_j)]\rangle = \int d\mathbf{r} \int d\mathbf{r'} \langle n(r)n(r')\rangle \exp[i\mathbf{Q}.(\mathbf{r}-\mathbf{r'})]$$

where summations or integrations are taken over all scatterers. The coherent scattering cross section is (as mentioned before):

$$d\sigma_c(Q)/d\Omega = \{b\}^2 S(Q). \qquad \text{(Eq. IX.4)}$$

Note that because coherent scattering is the only relevant part in our discussions, the subscript "c" will be dropped and the curly brackets around the coherent scattering length {b} will be omitted. Given these definitions, the various summations or integrations are usually split into two parts: one over scatterers that belong to the same macromolecule (intramolecular) and one that involves scatterer pairs belonging to different macromolecules (intermolecular). In the case of phase separated systems, the intra- and intermolecular pieces are replaced by intra- and interdomain contributions. The intramolecular part is often also referred to as single-"particle" as described in what follows for Gaussian coils and a few particle shapes.

IX. 2. Structure Factor for a Gaussian Coil

Consider a flexible polymer coil where each monomer pair located a distance $\mathbf{r}_{ij}$ apart obeys the Gaussian distribution:

$$P(\mathbf{r}_{ij}) = (3/2\pi\langle r_{ij}^2\rangle)^{3/2} \exp[-3r_{ij}/2\langle r_{ij}^2\rangle]. \qquad \text{(Eq. IX.5)}$$

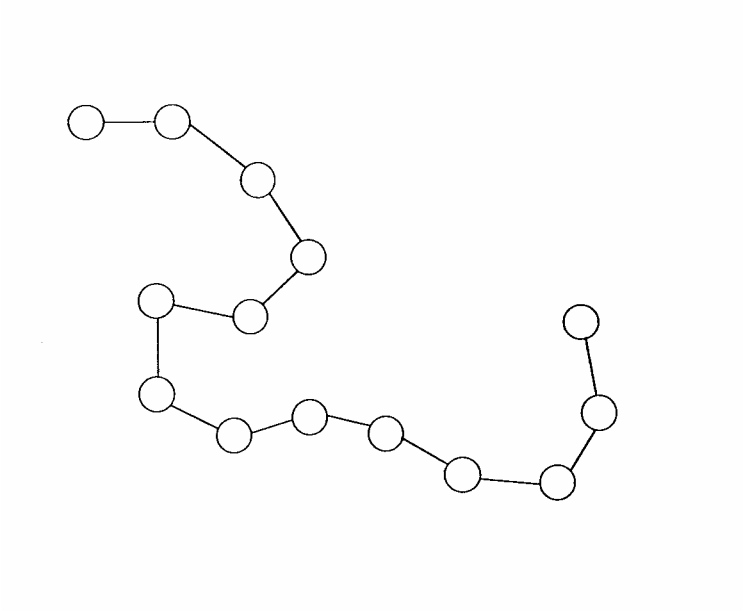

Figure IX.1: Schematic representation of a Gaussian coil.

The monomer pair is always correlated through chain connectivity so that the simplifying approximation $P(Q)=\{F(Q)\}^2$ (that will be made for uniform density objects) is not valid. The configuration average is taken over the probability distribution: $\langle ... \rangle = \int d\mathbf{r}_{ij}\, P(\mathbf{r}_{ij})$ ... and the static structure factor is given by:

$$P(Q) = (1/N^2) \sum_{ij}^{N} \langle \exp[-i\mathbf{Q}.\mathbf{r}_{ij}] \rangle = (1/N^2) \sum_{ij}^{N} \exp[-Q^2\langle r_{ij}^2\rangle/6] \qquad \text{(Eq. IX.6)}$$

where a property of the Gaussian distribution has been used:

$$\langle \exp[iQ_x x_{ij}] \rangle = \exp[-Q_x^2\langle x_{ij}^2\rangle/2] = \exp[-Q_x^2\langle r_{ij}^2\rangle/6]. \qquad \text{(Eq. IX.7)}$$

For a random walk chain, a further simplifying assumption is made: $\langle r_{ij}^2\rangle = a^2|i-j|$ where a is the so called statistical segment length and represents monomer size. To simplify the double summation, the following identity is used:

$$(1/N^2) \sum_{ij}^{N} F(|i-j|) = (1/N)F(0) + (2/N^2) \sum_{k}^{N} (N-k)F(k). \qquad \text{(Eq. IX.8)}$$

Furthermore, assuming that the degree of polymerization N (number of monomers per chain) is large compared to unity, P(Q) can be put into the form:

$$P(Q) = (2/N^2) \int_1^N dk\ (N-k)\ \exp(-Q^2a^2k/6) = 2 \int_0^1 dx\ (1-x)\ \exp(-Q^2a^2Nx/6).$$

The result is the well-known Debye function (Debye, 1947):

$$P(Q) = 2\ [\exp(-Q^2R_g^2)-1+Q^2R_g^2]/Q^4R_g^4 \qquad \text{(Eq. IX.10)}$$

where the radius of gyration is given by $R_g = (a^2N/6)^{1/2}$ and $(a^2N)^{1/2}$ represents the end-to-end distance. Small-Q and high-Q expansions of the Debye function are $P(QR_g<<1)=1-Q^2R_g^2/3$ and $P(QR_g>>1)=2/Q^2R_g^2$ respectively.

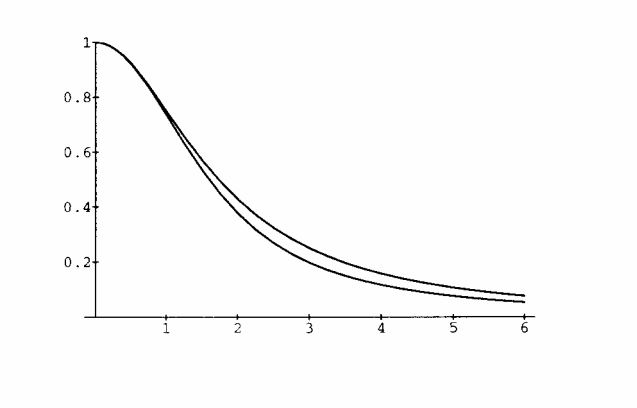

Figure IX.2. Variation of the Debye function $2[\exp(-X^2)-1+X^2]/X^4$ (bottom curve) and of a crude approximation to it $1/[1+X^2/3]$ (top curve) with the variable $X=Q^2R_g^2$.

Polymer chains follow Gaussian random walk statistics in polymer blends and in polymer solutions at the so-called theta temperature condition (where interactions between monomers and solvent are equivalent). Other structure factors are available for swollen chains (self-avoiding walk) or collapsed chains (self-attracting walk) in polymer solutions (for an overview, see for example Hammouda, 1993).

IX. 3. Other Polymer Chain Architectures

Many polymer chain architectures exist: "stars" consist of many equal size branches connected to a central core, "combs" consist of side branches grafted onto a main chain, "rings" consist of looped chains, "gels" consist of highly branched structures that are grown outwardly (dendrimers are the most regular gels), "networks" consist of crosslinked systems that contain a large number of interconnected structures, etc. These various polymer systems are made in the homopolymer form (all monomers are chemically identical) or copolymer form (each chain portion consists of blocks of monomers that are chemically different). Single-chain structure factors for such architectures have been worked out and are summarized elsewhere [Burchard, 1983; Hammouda, 1993]. In the remainder of this section, a systematic method based on multivariate Gaussian distributions used to calculate partial correlations for arbitrary architectures is described.

A simple case involving correlations between 2 blocks (n monomers each) separated by 3 linear chain portions (n_1, n_2 and n_3 monomers respectively) that are joined at the extremities of the 2 blocks (see Figure IX.3) is considered here. This structure can be constructed using a long linear chain (with $2n+n_1+n_2+n_3$ monomers) that comprises 2 crosslinks (corresponding to $\mathbf{r}_2=0$ and $\mathbf{r}_3=0$ in Figure IX.3). All segment lengths are assumed to be equal to a. A trivariate Gaussian distribution describing this structure is given by:

$$P(\mathbf{r}_1,\mathbf{r}_2,\mathbf{r}_3) = (3/2\pi a^2)^{9/2}\,\Delta^{-3/2}\exp\left[-(3/2a^2)\sum_{\mu,\nu=1}^{3}\mathbf{r}_\mu.D_{\mu\nu}.\mathbf{r}_\nu\right] \qquad \text{(Eq. IX.11)}$$

where $\mathbf{r}_1=\mathbf{r}_{ij}$, Δ is the determinant of the correlation matrix **C**, **D** is the inverse ($\mathbf{D}=\mathbf{C}^{-1}$) and the 9 elements of **C** are given by: $C_{\mu\nu} = \langle\mathbf{r}_\mu.\mathbf{r}_\nu\rangle/a^2$ with $\{\mu,\nu=1,3\}$. The formation of the two crosslinks (by setting $\mathbf{r}_2=\mathbf{r}_3=0$) leaves a univariate Gaussian distribution:

$$P(\mathbf{r}_1) = P(\mathbf{r}_1,0,0)\,/\int d^3r_1\,P(\mathbf{r}_1,0,0) \qquad \text{(Eq. IX.12)}$$

$$= (3/2\pi a^2)^{3/2}\,D_{11}{}^{3/2}\exp[-(3/2a^2)\,D_{11}\,r_1{}^2].$$

The average mean square distance between 2 monomers i and j that belong to the blocks of length n is therefore given by:

$$\langle r_{ij}{}^2\rangle/a^2 = 1/D_{11}. \qquad \text{(Eq. IX.14)}$$

More specifically:

$$\begin{aligned} C_{11} &= (n-i+j+n_1+n_2+n_3) \qquad \text{(Eq. IX.15)}\\ C_{12} &= C_{21} = (n_2+n_3)\\ C_{13} &= C_{31} = (n_1+n_2)\\ C_{22} &= (n_2+n_3)\\ C_{23} &= C_{32} = n_2\\ C_{33} &= (n_1+n_2) \end{aligned}$$

and therefore:

$$\langle r_{ij}{}^2\rangle = a^2\{(-i+j+n)(n_1n_2+n_1n_3+n_2n_3)+n_1n_2n_3\}/(n_1n_2+n_1n_3+n_2n_3). \qquad \text{(Eq. IX.16)}$$

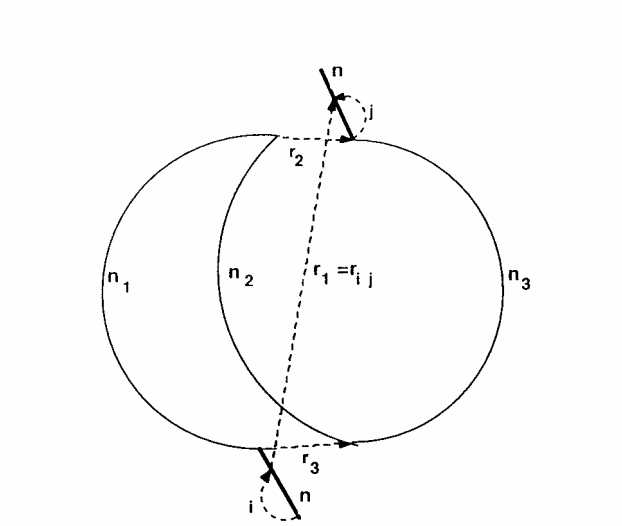

Figure IX.3: Correlations between two (outer) blocks in a particular polymer chain architecture.

The partial structure factor describing correlations between the two outside blocks is given by:

$$P(Q) = (1/n^2) \sum_{ij}^{n} \exp[-Q^2 \langle r_{ij}^2 \rangle /6] \qquad \text{(Eq. IX.17)}$$

which can be written simply as:

$$P(Q) = \exp[-Q^2a^2/6(1/n_1+1/n_2+1/n_3)]\{1-\exp[-Q^2a^2n/6]\}^2/[Q^2a^2n/6]^2. \qquad \text{(Eq. IX.18)}$$

In summary, this method consists in forming the correlation diagram using one single chain and choosing judiciously the location of crosslinks. All elements of the correlation matrix **C** need to be calculated so that the first element (recall that $\mathbf{r}_1=\mathbf{r}_{ij}$) of its inverse, $D_{11}=\Delta_{11}/\Delta$ (where Δ_{11} is the cofactor of element C_{11} and Δ is the determinant of **C**) is obtained therefore yielding $\langle r_{ij}^2 \rangle /a^2=\Delta/\Delta_{11}$. This procedure is useful for the calculation of correlations in many "lattice animals" needed in the modeling of complicated architectures (rings, "olympic rings", regular networks, etc).

IX. 4. Structure Factor for a Uniform Sphere

Consider a sphere of radius R and uniform density (this could be a spherical domain in a microphase separated block copolymer or a latex particle in a colloidal suspension). The single particle structure factor P(Q) involves integrations over the volume V of the sphere (in spherical coordinates):

$$P(Q) = \langle n(-Q)n(Q) \rangle /N^2 = \int d\mathbf{r} \int d\mathbf{r'} \exp[i\mathbf{Q}.(\mathbf{r}-\mathbf{r'})] \langle n(r)n(r') \rangle /N^2. \qquad \text{(Eq. IX.19)}$$

Because the scattering elements are not correlated, the average of the product <n(r)n(r')> is equal to the product of the averages <n(r)><n(r')> and therefore:

$$P(Q) = |F(Q)|^2 \qquad \text{(Eq. IX.20)}$$

where the form factor is: $F(Q) = \int d\mathbf{r} \exp[i\mathbf{Q}.\mathbf{r}] \langle n(r)\rangle/N$. For uniform density, the average over configurations <n(r)> becomes trivial:

$$\begin{aligned} \langle n(r)\rangle &= N/V = n \quad && \text{if } r \le R \\ \langle n(r)\rangle &= 0 && \text{if } r > R \end{aligned} \qquad \text{(Eq. IX.21)}$$

so that:

$$F(Q) = (3/4\pi R^3) \int_0^R r^2 dr \int_{-1}^{1} d\mu \exp[iQr\mu] \int_0^{2\pi} d\phi \qquad \text{(Eq. IX.22)}$$

$$= (3/R^3) \int_0^R r^2 dr \, [\sin(Qr)/(Qr)] = 3j_1(QR)/(QR) \qquad \text{(Eq. IX.23)}$$

where the spherical Bessel function $j_1(x)$:

$$j_1(x) = \sin(x)/x^2 - \cos(x)/x = (\pi/2x)^{1/2} J_{3/2}(x) \qquad \text{(Eq. IX.24)}$$

has been used. The structure factor for the sphere is therefore:

$$P(Q) = [3j_1(QR)/(QR)]^2 = \{3[\sin(QR)/(QR)^2 - \cos(QR)/(QR)]/(QR)\}^2 . \qquad \text{(Eq. IX.25)}$$

Note that by normalization P(Q=0)=1. Similarly to the calculation of the single-particle structure factor, one can calculate a radius of gyration (squared):

$$R_g^2 = \int d\mathbf{r} \int d\mathbf{r'} \langle(\mathbf{r}-\mathbf{r'})^2\rangle = (3/4\pi R^3) \int_0^R dr \, 4\pi r^4 = 3R^2/5 \qquad \text{(Eq. IX.26)}$$

The Guinier (Q->0) expansion gives: $P(Q) \to 1 - Q^2R_g^2/3 + Q^4R_g^4/12 + \ldots$ (Eq. IX.27)

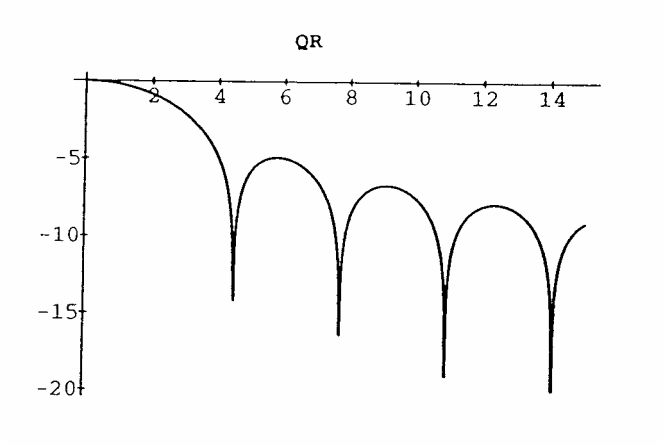

Figure IX.4: Plot of Log(P(Q)) vs QR for a uniform sphere showing many order oscillations.

IX. 5. Structure Factors for Other Spheroid Shapes

Following the same procedure, the form factor and structure factor for a spherical shell between radii R_1 and R_2 (and hollow for $r<R_1$) can be calculated as follows:

$$F(Q) = \{3/4\pi(R_2^3-R_1^3)\} \int_{R_1}^{R_2} r^2 dr \int_{-1}^{1} d\mu \exp[iQr\mu] \int_{0}^{2\pi} d\phi \qquad \text{(Eq. IX.28)}$$

$$P(q) = \{3j_1(QR_2)R_2^3/(QR_2)-3j_1(QR_1)R_1^3/(QR_1)\}^2/\{R_2^3-R_1^3\}^2. \qquad \text{(Eq. IX.29)}$$

The radius of gyration (squared) for the spherical shell is

$$R_g^2 = \{3/4\pi(R_2^3-R_1^3)\} \int_{R_1}^{R_2} dr\, 4\pi r^4 = 3(R_2^5-R_1^5)/5(R_2^3-R_1^3) \qquad \text{(Eq. IX.30)}$$

For an ellipsoid of half axes a, b, c oriented so that its axes make angles α, β, γ with the **Q** direction, an effective radius R_e is defined as:

$$R_e^2=a^2\cos^2(\alpha)+b^2\cos^2(\beta)+c^2\cos^2(\gamma). \qquad \text{(Eq. IX.31)}$$

The form factor is the same as the one for a sphere of radius R_e:

$$F(Q) = 3j_1(QR_e)/(QR_e) \qquad \text{(Eq. IX.32)}$$

and the structure factor (for a randomly oriented sample) is an average over all possible orientations of the ellipsoid.:

$$P(q) = \int_0^{\pi/2} d\gamma \sin(\gamma) \{F(Q)\}^2 \qquad \text{(Eq. IX.33)}$$

where γ is the angle between the major axis of the ellipsoid and the **Q** direction. It is straightforward to extend these results to an ellipsoidal shell.

IX. 6. Structure Factors for Cylindrical Shapes

The form factor F(Q) for a uniform cylinder (rod) of radius R and length L oriented at an angle γ from the **Q** direction is the product of a longitudinal ($\Uparrow$ along the rod) and a transverse ($\perp$ perpendicular to the rod) contributions in cylindrical coordinates:

$$F(Q,\gamma) = [1/\pi R^2 L] \int_{-L/2}^{L/2} dr_{\Uparrow} \exp[iQr_{\Uparrow} \cos(\gamma)] \int_0^R dr_{\perp}\, r_{\perp} \int_0^{2\pi} d\phi \exp[iQr_{\perp}\cos(\phi)\sin(\gamma)] \,.$$

The $r_{\square}$ integral can be written as:

$$[1/\pi R^2] \int_0^R dr_{\perp}\, r_{\perp} \int_0^{\pi} d\phi \cos[Qr_{\perp} \cos(\phi)\sin(\gamma)] \,. \qquad \text{(Eq. IX.35)}$$

and can be reduced to give the result:

$$F(Q,\gamma) = \{\sin[QL\cos(\gamma)/2]/[QL\cos(\gamma)/2]\} \{2J_1[QR\sin(\gamma)]/[QR\sin(\gamma)]\} \qquad \text{(Eq. IX.36)}$$

where:

$$J_1(x) = [1/\pi] \int_0^{\pi} d\phi \cos(\phi) \exp[ix\cos(\phi)] \qquad \text{(Eq. IX.37)}$$

is the cylindrical Bessel function of first order. Note that the first term $j_0(QL\cos(\gamma)/2) = \{\sin[QL\cos(\gamma)/2]/[QL\cos(\gamma)/2]\}$ is the spherical Bessel function of order zero (lower case j's represent spherical and capital J's represent cylindrical Bessel functions). The structure factor involves the final orientational averaging for randomly oriented rods:

$$P(Q) = \int_0^{\pi/2} d\gamma \sin\gamma \{F(Q,\gamma)\}^2. \qquad \text{(Eq. IX.38)}$$

In order to model the scattering from very dilute solutions of rods (for example lyotropic liquid crystal polymers in the low-concentration isotropic phase), the remaining integral (over γ) is

performed numerically. For oriented samples (for example in a shear or magnetic field) this averaging over γ's is not necessary.

The radius of gyration (squared) is given by similar integrals where the phase factor exp[i**Q.r**] is replaced by $r^2=r_{\Uparrow}^2+ r_{\perp}^2$. The result is: $R_g^2 = L^2/12+R^2/2$.

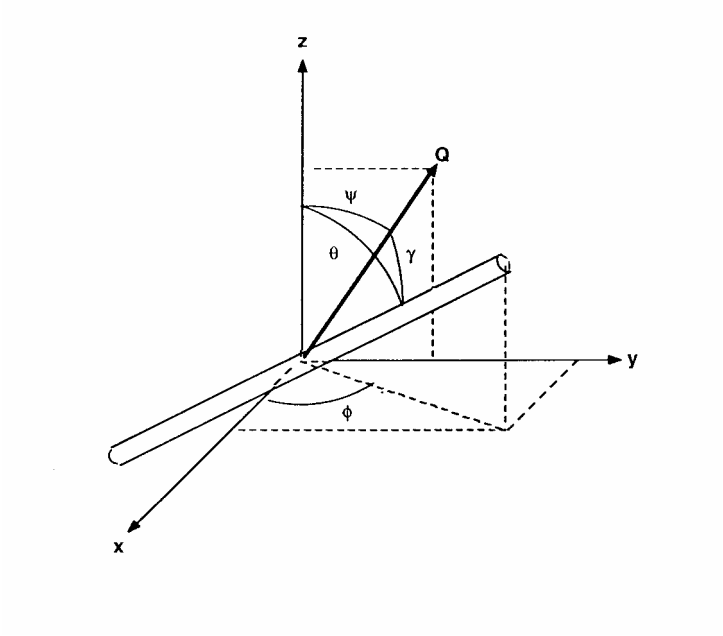

Figure IX.5.Geometry of the uniform rod.

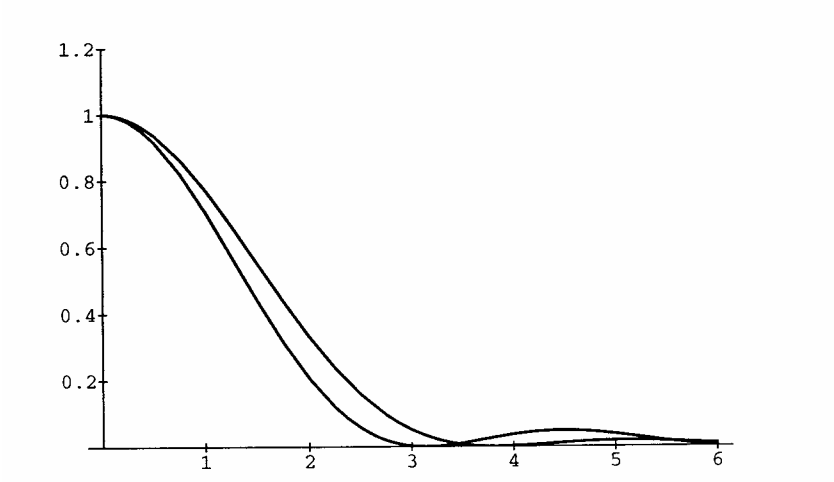

Figure IX.6. Plots of the two functions $[2J_1(X)/X]^2$ and $[\sin(X)/X]^2$ that give the variations of the structure factor perpendicular to the rod axis and along its direction.

For a disk of radius R and negligible thickness, the L->0 limit in the general result is taken so that:

$$F(Q,\gamma) = (1/\pi R^2) \int_0^R rdr \int_0^{2\pi} d\phi \exp[iQr \sin(\gamma)\cos(\phi)] \qquad \text{(Eq. IX.39)}$$

and the final result is:

$$P(Q) = (2/Q^2R^2)[1-J_1(2QR)/QR]. \qquad \text{(Eq. IX.40)}$$

The radius of gyration of a disk is: $R_g=R/(2)^{1/2}$.

To obtain the structure factor for an infinitely thin rod of length L, we take the R->0 limit instead, and obtain:

$$P(Q) = \int_0^{\pi/2} d\gamma \sin(\gamma) \{\sin[QL\cos(\gamma)/2]/[QL\cos(\gamma)/2]\}^2 \qquad \text{(Eq. IX.41)}$$

$$= (2/QL)\, Si(QL) - \sin^2(QL/2)/(QL/2)^2$$

where Si(x) is the sine integral defined as:

$$Si(x) = \int_0^x du \sin(u)/u \qquad \text{(Eq. IX.42)}$$

The radius of gyration for an infinitely thin rod is: $R_g=L/(12)^{1/2}$.

IX. 7. Pair Correlation Functions

The structure factor S(Q) is the Fourier transform of the probability distribution function P(**r**):

$$S(Q) = \int d\mathbf{r} \exp[i\mathbf{Q}.\mathbf{r}]\, P(\mathbf{r}) . \qquad \text{(Eq. IX.43)}$$

Given an infinitesimal scattering volume chosen randomly in the considered "particle", P(**r**) represents the probability of finding another scatterer within the particle a distance **r** apart. Usually, a one-dimensional probability distribution p(r) (also referred to as "distance distribution function") is defined instead:

$$S(Q) = (1/R) \int_0^R dr\, [\sin(Qr)/(Qr)]\, p(r). \qquad \text{(Eq. IX.44)}$$

p(r) is available for some of the shapes discussed before. For a sphere of radius R:

$$p(r) = 12(r/2R)^2[1-r/2R]^2(2+r/2R)$$
$$= 3(r/R)^2[1-3r/4R+r^3/16R^3] \qquad \text{(Eq. IX.45)}$$

For a disk of radius R:

$$p(r) = (8r/\pi R)\{\arccos(r/2R)-(r/2R)[1-(r/2R)^2]^{1/2}\} \qquad \text{(Eq. IX.46)}$$

For an infinitely thin rod of length L, the integration is performed from 0 to L instead, the normalization constant is 1/L and:

$$p(r) = 2[1-r/L]. \qquad \text{(Eq. IX.47)}$$

Note that the probability distribution function P(**r**) is better known when defined for "interparticle" contributions (correlations in a "liquid" of point particles) and is often referred to as pair correlation function g(**r**)=VP(**r**) (where V is the sample volume):

$$S(Q) = (1/V) \int d\mathbf{r} \exp[i\mathbf{Q}.\mathbf{r}] [g(\mathbf{r})-1] . \qquad \text{(Eq. IX.48)}$$

where a constant term that has no contribution except in the forward direction ($\int d\mathbf{r} \exp[i\mathbf{Q}.\mathbf{r}] = (2\pi)^3\delta(\mathbf{Q})$) has been added.

IX. 8. Structure Factor for a Parallelepipedon

Even though this is not a realistic shape to describe material microstructures in the nanometer scale, it is included here for completeness. Consider a rectangular parallelepipedon of sides a, b, c. In cartesian coordinates, the form factor can be split into the product of three pieces that depend on the three coordinates respectively:

$$F(Q_x,Q_y,Q_z) = [1/abc] \int_{-a/2}^{a/2} dx \exp[iQ_x x] \int_{-b/2}^{b/2} dy \exp[iQ_y y] \int_{-c/2}^{c/2} dz \exp[iQ_z z] \qquad \text{(Eq. IX.49)}$$

$$= [\sin(Q_x a/2)/(Q_x a/2)] [\sin(Q_y b/2)/(Q_y b/2)] [\sin(Q_z c/2)/(Q_z c/2)]$$

and the structure factor is, here also, an average over orientations:

$$P(Q_x,Q_y,Q_z) = \int_0^{\pi/2} d\gamma \sin\gamma \{F(Q_x,Q_y,Q_z)\}^2. \qquad \text{(Eq. IX.50)}$$

where γ is the orientation angle between **Q** and one of the symmetry axes of the parallelepipedon.

References

O. Kratky and G. Porod, "Diffuse Small-Angle X-rays in Colloid Systems", J. of Colloid and Interface Science 4, 35 (1949)

W. Burchard, "Static and Dynamic Light Scattering from Branched Polymers and Biopolymers", Advances in Polymer Science 48, 1 (1983)

B. Hammouda, "SANS from Homogeneous polymer Mixtures: A Unified Overview", Advances in Polymer Science 106, 87 (1993)

J.S. Higgins and H. Benoit, "Polymers and Neutron Scattering", Oxford (1994)

M. Abromowitz and I.A. Stegun, "Handbook of Mathematical Functions", Dover Publications (1965)

IX. 9. Questions

1. What is the high-Q expansion of the Debye function (structure factor for Gaussian coil)?
2. What standard plot is used to obtain the radius of gyration? the correlation length? the persistence length?
3. Look up the spherical and cylindrical Bessel functions in a Math book (Abromowitz and Stegun for example). How are they related?
4. Look up the structure factor for star branched polymers (Higgins and Benoit, 1994, for example). What is its high Q expansion?
5. SANS from isolated spherical objects (dilute solution of latex particles for example) is characterized by oscillation. Are these oscillations always observed experimentally?
6. Could one obtain a peak from single-particle scattering?
7. Derive the probability distribution function $p(r) = 12(r/2R)^2[1-r/2R]^2(2+r/2R)$ for a sphere (look up Kratky-Porod, 1949).
8. Rederive the structure factor for a sphere on your own.
9. Familiarize yourself with the procedure to calculate partial structure factors for block copolymers (look up Hammouda, 1993 for example) for example.
10. Using the multivariate method described in these notes, work out the structure factor for a Gaussian ring.

X. INTERCHAIN AND INTERPARTICLE STRUCTURE FACTORS

Except at the infinite dilution limit, interchain and interparticle contributions have to be included in any description of the scattering from polymer systems.

X. 1. Case of a Polymer Melt

Consider a homopolymer melt consisting of M chains of degree of polymerization N each. The structure factor S(Q) can be split into an intrachain part and an interchain part:

$$S(Q) = \sum_{\alpha}^{M} \sum_{ij}^{N} \langle \exp[i\mathbf{Q}.\mathbf{r}_{\alpha i \alpha j}] \rangle + \sum_{\alpha, \beta \neq \alpha}^{M} \sum_{ij}^{N} \langle \exp[i\mathbf{Q}.\mathbf{r}_{\alpha i \beta j}] \rangle \qquad \text{(Eq.X.1)}$$

$$= MN^2P(Q) + M(M-1)N^2R(Q)$$

where $\mathbf{r}_{\alpha i \beta j}$ is the interdistance between a pair of monomers i and j belonging to two polymer chains α and β, P(Q) is the single-chain structure factor and R(Q) is the inter-chain structure factor:

$$P(Q) = (1/N^2) \sum_{ij}^{N} \langle \exp[i\mathbf{Q}.\mathbf{r}_{1i1j}] \rangle \qquad \text{(Eq. X.2a)}$$

$$R(Q) = (1/N^2) \sum_{ij}^{N} \langle \exp[i\mathbf{Q}.\mathbf{r}_{1i2j}] \rangle \qquad \text{(Eq. X.2b)}$$

where we have chosen a pair of chains 1 and 2 and summed over the M(M-1) possible pairs. Because M>>1, M(M-1) can be approximated by M^2.

X. 2. Case of a Homogeneous Mixture of Deuterated and Nondeuterated Polymers

In the case of a homogeneous mixture of deuterated and nondeuterated polymers that are identical except for deuteration, the intrachain structure factor P(Q) and interchain structure factor R(Q) are assumed to be independent of isotope (deuteration) effect; this assumes that deuteration does not change chain conformations and monomer interactions. For incompressible homogeneous mixtures, the fluctuating densities compensate each other ($\Delta n_H(Q) + \Delta n_B(Q) = 0$) so that the various partial structure factors are related:

$$S_{DD}(Q) = \langle n_D(-Q) n_D(Q) \rangle = -S_{DH}(Q) = S_{HH}(Q). \qquad \text{(Eq. X.3)}$$

They can be expressed as:

$$S_{DD}(Q) = M_D N^2 P(Q) + M_D^2 N^2 R(Q) \qquad \text{(Eq. X.4)}$$
$$S_{HH}(Q) = M_H N^2 P(Q) + M_H^2 N^2 R(Q)$$
$$S_{DH}(Q) = M_D M_H N^2 R(Q)$$

where M_D and M_H are the number of deuterated and undeuterated chains respectively and N is the degree of polymerization of all chains. Setting $S_{DD}(Q) + S_{DH}(Q) = 0$ (incompressibility) yields: $M_D N^2 P(Q) + M_D(M_D+M_H) N^2 R(Q) = 0$. This example shows one method of expressing the interchain contribution R(Q) in terms of the intrachain part P(Q) as:

$$R(Q) = -P(Q)/(M_D+M_H). \qquad \text{(Eq. X.5)}$$

Using this expression, one obtains:

$$S_{DD}(Q) = [M_D M_H/(M_D+M_H)]\, N^2 P(Q) \qquad \text{(Eq. X.6)}$$

and the cross section (for the whole sample) is given by:

$$d\sigma(Q)/d\Omega = b_D^2\, S_{DD}(Q) + b_H^2\, S_{HH}(Q) + 2 b_D b_H\, S_{DH}(Q) \qquad \text{(Eq. X.7)}$$

$$= (b_D - b_H)^2\, S_{DD}(Q)$$

where the coherent scattering lengths for the deuterated and nondeuterated monomers b_D and b_H have been used to form the contrast factor $(b_D-b_H)^2$.

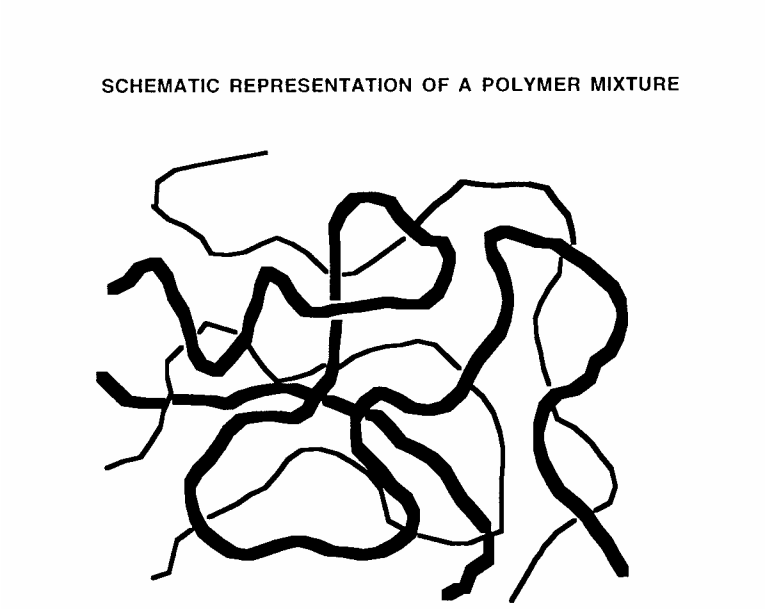

Figure X.1: Schematic representation for a mixture of deuterated and nondeuterated polymers (deuteration is assumed not to affect chain conformations and monomer interactions).

X. 3. Case of a Dilute Polymer Solution

Another well known mean field approximation used to express the interchain part R(Q) in terms of the single chain part P(Q) is called Zimm's single-contact approximation (Zimm, 1946) which assumes that two polymer chains in dilute solution can interact only through one effective contact. Consider two monomers (call them i and j) on two neighboring chains (say chains 1 and 2) and write their interdistance vector as: $\mathbf{r}_{1i2j} = \mathbf{r}_{1i1k} + \mathbf{r}_{1k2m} + \mathbf{r}_{2m2j}$ where k-m is the single-contact between the two chains. With this approximation, the interchain structure factor can be simplified:

$$\sum_{ij}^{N} <\exp[i\mathbf{Q}.\mathbf{r}_{1i2j}]> = \sum_{ij}^{N} <\exp[i\mathbf{Q}.\mathbf{r}_{1i1k}]> <\exp[i\mathbf{Q}.\mathbf{r}_{1k2m}]> <\exp[i\mathbf{Q}.\mathbf{r}_{2m2j}]> . \quad \text{(Eq. X.8)}$$

This decoupling of the three terms is possible only because the probability densities can be written as products:

$$P(\mathbf{r}_{1i},\mathbf{r}_{1k},\mathbf{r}_{2m}) = P(\mathbf{r}_{1i},\mathbf{r}_{1k})P(\mathbf{r}_{1k},\mathbf{r}_{2m})P(\mathbf{r}_{2m},\mathbf{r}_{2j}). \quad \text{(Eq. X.9)}$$

The $<\exp[i\mathbf{Q}.\mathbf{r}_{1k2m}]>$ term is the excluded volume between the two polymer chains and is defined as v (normalized to the sample volume V):

$$v/V = -\int d\mathbf{r}_{1k2m}\,[g(\mathbf{r}_{1k2m})-1]\exp[i\mathbf{Q}.\mathbf{r}_{1k2m}] = -\langle\exp[i\mathbf{Q}.\mathbf{r}_{1k2m}]\rangle \quad \text{(Eq. X.10)}$$

so that R(Q) becomes:

$$N^2R(Q) = -(v/V)\,[N^2P(Q)]^2 \quad \text{(Eq. X.11)}$$

This formula:

$$S(Q) = MN^2P(Q) - (v/V)\,[MN^2P(Q)]^2 \quad \text{(Eq. X.12)}$$

is valid for very dilute solutions whereby interchain contributions are weak (equivalent to keeping only the second virial coefficient in a virial expansion).

Higher order contributions (see Higgins-Benoit, 1994 for example) describing interactions between two chains through a third chain are taken into account by adding $(v/V)^2[MN^2P(Q)]^3$, or in general through n intermediate chains by adding $(v/V)^{n-1}[MN^2P(Q)]^n$:

$$S(Q) = MN^2P(Q) - (v/V)[MN^2P(Q)]^2 + (v/V)^2[MN^2P(Q)]^3 + (v/V)^3[MN^2P(Q)]^4 + \ldots \quad \text{(Eq. X.13)}$$

This series can actually be re-summed ($1-x+x^2-x^3+\ldots=1/1+x$) to give:

$$S(Q) = MN^2P(Q)/[1 + (v/V)MN^2P(Q)] \text{ or } S^{-1}(Q) = 1/MN^2P(Q) + v/V \quad \text{(Eq. X.14)}$$

which is the basis for the Zimm plot. This mean field result applies for non-dilute solutions as well. In fact, it works better for semidilute and concentrated solutions because the types of interactions that are not included (loop interactions within a chain and multiple contact interactions) become smaller when the polymer concentration increases. When such interactions are important (in dilute solutions), renormalization group theories do a better job at describing polymer solutions.

Defining a more practical variable for the polymer volume fraction $\phi=MNv_0/V$ where v_0 is the monomer molar volume, MN is the total number of monomers in the solution and V is the sample volume and redefining the structure factor as $S(Q)=S(Q)v_0^2/V$ (the reason for this normalization will become apparent in the next section), we obtain:

$$\phi/S(Q) = 1/Nv_0P(Q) + (v/v_0)\phi \quad \text{(Eq. X.15)}$$

Using the small-Q expansion ($1/P(Q)\to 1+Q^2R_g^2/3$), one can see that a plot of $\phi/S(Q)$ vs Q^2 yields $R_g^2/3$ as slope and $(1/N)+(v/v_0)\phi$ (degree of polymerization and excluded volume) as intercept. The excluded volume v is related to the second virial coefficient A_2 as:

$$v = 2\,A_2\,m_w^2/N_{av} \quad \text{(Eq. X.16)}$$

where m_w is the monomer molar mass and N_{av} is Avogadro's number.

The macroscopic cross section is given by:

$$d\Sigma(Q)/d\Omega = (b_p/v_p-b_s/v_s)^2S(Q) \quad \text{(Eq. X.17)}$$

where the contrast factor contains the monomer and solvent scattering lengths b_p and b_s respectively and molar volumes v_p and v_s. Note that the macroscopic cross section $d\Sigma(Q)/d\Omega$ is obtained by multiplying the monomer number density MN/V by the microscopic cross section per monomer (1/MN) $d\sigma(Q)/d\Omega$.

X. 4. Case of a Homopolymer Blend Mixture (the Random Phase Approximation formula)

Consider an incompressible mixture consisting of two different polymers A and B with degrees of polymerization N_A and N_B, radii of gyration R_{gA} and R_{gB}, compositions ϕ_A and ϕ_B and molar volumes v_A and v_B. The random phase approximation (RPA also called the de Gennes formula) has been discussed extensively elsewhere and will be summarized here only (de Gennes, 1979): The structure factor for the fully interacting blend is given by:

$$1/S_{AA}(Q) = 1/S_{AA}^{0}(Q) + 1/S_{BB}^{0}(Q) - 2\,\chi_{AB}/v_0 \qquad \text{(Eq. X.18)}$$

where the "bare" (noninteracting) system structure factors have been defined:

$$S_{AA}^{o}(Q) = N_A\phi_A v_A P_A(Q) \qquad \text{(Eq. X.19)}$$
$$S_{BB}^{o}(Q) = N_B\phi_B v_B P_B(Q)$$
$$P_J(Q) = 2\,[\exp(-Q^2 R_{gJ}^2)-1+Q^2 R_{gJ}^2]/(Q^4 R_{gJ}^4],\ J=(A,B)$$

$P_A(Q)$ and $P_B(Q)$ are the single-chain structure factors (Debye function) discussed previously and v_0 is a "reference" volume (taken to be $v_0=(v_A v_B)^{1/2}$). The Flory-Huggins interaction "chi" parameter, χ_{AB}, is given in terms of the monomer-monomer interaction potentials W_{AA}, W_{BB}, W_{AB} and the sample temperature k_BT as:

$$\chi_{AB} = [W_{AB}-(W_{AA}+W_{BB})]/k_BT. \qquad \text{(Eq. X.20)}$$

The coherent scattering (macroscopic) cross section is given by:

$$d\Sigma(Q)/d\Omega = (b_A/v_A)^2 S_{AA}(Q) + (b_B/v_B)^2 S_{BB}(Q) + 2(b_A b_B/v_A v_B)S_{AB}(Q) \qquad \text{(Eq. X.21)}$$

which can be reduced to:

$$d\Sigma(Q)/d\Omega = (b_A/v_A-b_B/v_B)^2\, S_{AA}(Q) \qquad \text{(Eq. X.22)}$$

for incompressible systems (where $S_{AA}(Q)=-S_{AB}(Q)=S_{BB}(Q)$). Here also, we find that the scattered intensity is the product of a contrast factor and a structure factor, but this time, the structure factor contains interparticle contributions.

X. 5. Multicomponent Homogeneous Polymer Mixture

Consider a mixture of homopolymers and block copolymers with an arbitrary number n of components (note that here a diblock copolymer is referred to as a two-component system).

Each component (say A) is characterized by an "ideal" structure factor $S_{AA}^0(Q)$; block copolymers (say B-C) are even characterized by cross structure factors $S_{BC}^0(Q)$; and monomer-monomer interactions (say A/B) are described by Flory-Huggins interaction parameters χ_{AB}. Following a standard method, one chooses one of the homopolymers as a reference component (say A) so that the incompressible multicomponent random phase approximation result (generalization of the de Gennes formula) can be presented in a generalized matrix form (Akcasu, 1992):

$$\boldsymbol{S}^{-1}(Q) = \boldsymbol{S}_0^{-1}(Q) + \mathbf{v}/v_0^2 \qquad \text{(Eq. X.23)}$$

where the (n-1)x(n-1) components of matrix $\boldsymbol{S}_0(Q)$ are the various ideal structure factors $S_{BC}^0(Q)$, etc, and the various excluded volumes are:

$$v_{BB}/v_0^2 = 1/S_{AA}^0(Q) - 2\chi_{BA} \qquad \text{(Eq. X.24)}$$
$$v_{CC}/v_0^2 = 1/S_{AA}^0(Q) - 2\chi_{CA}$$
$$v_{BC}/v_0^2 = 1/S_{AA}^0(Q) + \chi_{BC} - \chi_{BA} - \chi_{CA} .$$

Note that for notation convenience, we will redefine the excluded volumes as: $V_{BB}=v_{BB}/v_0^2$.

This method is implemented here for an incompressible ternary blend mixture (A/B/C) in the homogeneous phase region. The three independent structure factors are given by:

$$S_{AA}(Q) = S_{AA}^o[1+V_{BB}S_{BB}^o]/Den \qquad \text{(Eq. X.25)}$$
$$S_{BB}(Q) = S_{BB}^o[1+V_{AA}S_{AA}^o]/Den$$
$$S_{AB}(Q) = -S_{AA}^oV_{AB}S_{BB}^o/Den$$

and the denominator is: $Den = [(1+V_{AA}S_{AA}^o)(1+V_{BB}S_{BB}^o)-V_{AB}^2S_{AA}^oS_{BB}^o]$. The spinodal line is obtained by setting Den=0.

X. 6. The Ornstein-Zernike Equation

Interparticle interferences for various sample morphologies (in phase separated block copolymers or in colloidal suspensions for example) are modeled using an equation that found wide use in another area of research (wide-angle scattering from liquids and liquid mixtures). The Ornstein-Zernike equation (Ornstein-Zernike, 1918) relates the total correlation function h(r) = g(r) - 1 to the direct correlation function c(r) through an integral equation, which for structureless particles can be written as:

$$h(r) = c(r) + m \int dr'\, c(r-r')h(r'). \qquad \text{(Eq. X.26)}$$

where m is the particle number density. The first term on the RHS represents direct binary interactions between two particles whereas the second term represents three-body and higher order interactions. The pair correlation function g(r) is related to the interparticle interaction potential U(r) as:

$$g(r) = \exp[-U(r)/k_BT] \qquad \text{(Eq. X.27)}$$

where k_BT is the sample temperature in energy units. Because the potential of mean-force U(r) contains contributions from many-body interactions, it is expanded in terms of binary (w_{ij}), ternary (w_{ijk}), and higher order interactions:

$$U(r) = \sum_{ij} w_{ij}(r) + \sum_{ijk} w_{ijk}(r) + \text{etc.} \qquad \text{(Eq. X.28)}$$

Our dilemma is that we have one integral equation (Ornstein-Zernike) with two unknowns (h(r) and c(r)); this can be solved only if another (so called "closure") relation is introduced. Many of these closure relations have been discussed (hypernetted chains, Born-Green, Percus-Yevick, mean spherical approximation, etc). Using these closure relations, numerical solutions of the Ornstein-Zernike equation yield realistic interparticle structure factors (Schweizer-Curro, 1989) . The last two closure relations (Percus-Yevick and mean spherical approximations) are discussed here because they allow simple analytical solutions to the integral equation.

X. 7. The Percus-Yevick Approximation

This approximation gives another relation in order to "close" the integral equation:

$$c(r) = g(r)[1-\exp[-w(r)/k_BT] \qquad \text{(Eq. X.29)}$$

which, for a hard sphere interaction potential between particles:

$$w(r) = 0 \text{ for } r>\sigma \qquad \text{(Eq. X.30)}$$
$$w(r) = \infty \text{ for } r<\sigma$$

gives the solution:

$$c(r) = 0 \text{ for } r>\sigma \qquad \text{(Eq. X.31)}$$
$$c(r) = -\lambda_1-6\phi\lambda_2 r/\sigma-(\phi/2)\,\lambda_1 r^3/\sigma^3 \text{ for } r<\sigma$$

where:

$$\lambda_1 = (1+2\phi)^2/(1-\phi)^4 \text{ and } \lambda_2 = -(1+\phi/2)^2/(1-\phi)^4 \qquad \text{(Eq. X.32)}$$

ϕ is the packing fraction ($=\pi m\sigma^3/6$), m is the density of scattering particles and σ is the "effective" particle diameter.

The Fourier transform of the direct correlation function can be calculated as:

$$C(Q) = -24\phi\,\{\lambda_1\,[\sin(Q\sigma)-(Q\sigma)\cos(Q\sigma)]/(Q\sigma)^3 -$$
$$6\phi\,\lambda_2\,[(Q\sigma)^2\cos(Q\sigma)-2(Q\sigma)\sin(Q\sigma)-2\cos(Q\sigma)+2]/(Q\sigma)^4 -$$
$$(\phi\lambda_2/2)\,[(Q\sigma)^4\cos(Q\sigma)-4(Q\sigma)^3\sin(Q\sigma)-$$
$$12(Q\sigma)^2\cos(Q\sigma)+24(Q\sigma)\sin(Q\sigma)+24\cos(Q\sigma)-24]/(Q\sigma)^6\} \qquad \text{(Eq. X.33)}$$

and the structure factor for a liquid of structureless particles is given by:

$$S^{-1}(Q) = 1 - C(Q) \qquad \text{(Eq. X.34)}$$

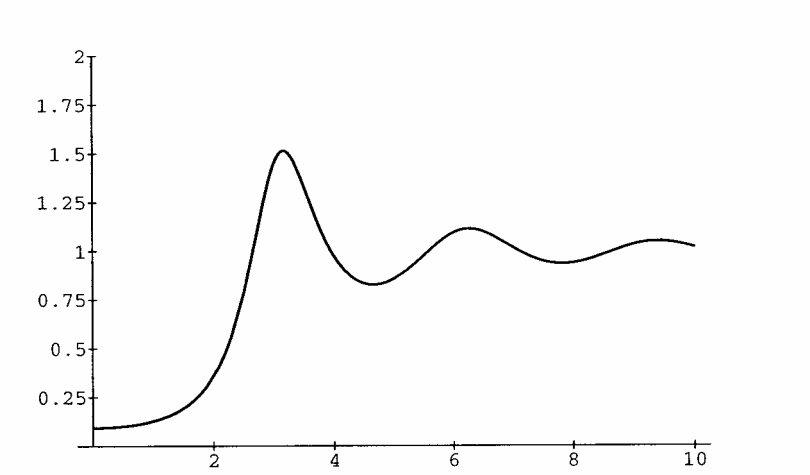

Figure X.2: Pure interparticle structure factor S(QR) vs QR prediction from the Percus-Yevick model (with hard sphere potential) for ϕ=0.30 (note that R=σ/2).

In order to include intraparticle structure, the following form is used instead:

$$S^{-1}(Q) = S_0^{-1}(Q) - C(Q) \qquad \text{(Eq. X.35)}$$

where $S_0(Q)$ is the single particle structure factor ($S_0(Q)=\phi v_0 P(Q)$).

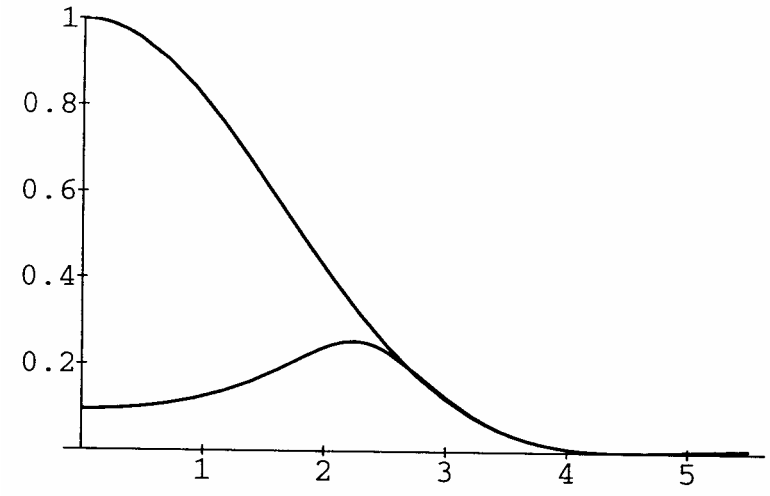

Figure X.3: Structure factors for isolated spheres (infinite dilution limit), and for a concentrated sphere mixture containing both interparticle (Percus-Yevick with hard sphere potential) and intraparticle (uniform density sphere) for ϕ=0.30.

X. 8. The Mean Spherical Approximation

This simple approximation assumes that: $c(r) = -w(r)/k_BT$. Because (as will be shown here) this approximation is the mean field approximation for polymer systems described previously, intraparticle contributions are included in the Ornstein-Zernike equation (from the outset) which becomes (in Fourier space):

$$H(Q) = -S_0(Q)W(Q)S_0(Q)/k_BT - [M/V]S_0(Q)W(Q)H(Q)/k_BT \qquad \text{(Eq. X.36)}$$

where M/V is the total number of "particles" (think polymer chains) per unit volume. After recognizing that $S(Q) = S_0(Q) + [M(M-1)/V]H(Q)$, one obtains:

$$S^{-1}(Q) = S_0^{-1}(Q) + W(Q)/k_BT \qquad \text{(Eq. X.37)}$$

which is the random phase approximation result obtained for polymer solutions (where the intermonomer potential W/k_BT is replaced by the excluded volume v/V) and for polymer blends (where W/k_BT is replaced by $1/S_{BB}^0(Q) - 2\chi_{AB}/v_0$).

Note that because the mean field approximation does not model the local interactions (for interparticle interdistances smaller than particle sizes) properly, packing effects (on thermodynamics and phase separation for example) are neglected. For this reason, the g(r) obtained from such mean field theories does not show realistic oscillations for the neighboring coordination shells. The appeal of this approach is the fact that it gives simple analytical results.

References

A.Z. Akcasu in "Dynamic Light Scattering: The Method and Some Applications", W. Brown, Editor, Oxford Press, (1992).

P. Debye, J. Phys. Colloid. Chem. 51, 18 (1947)

K.S. Schweizer and J. Curro, J. Chem. Phys. 91, 256 (1989)

P.G. de Gennes, "Scaling Concepts in Polymer Physics", Cornell University Press, New York (1979)

B. Hammouda, "SANS from Homogeneous polymer Mixtures: A Unified Overview", Advances in Polymer Science 106, 87 (1993)

J.P. Hansen and I.R. McDonald, "Theory of Simple Liquids" Academic Press, London (1986)

J.S. Higgins and H. Benoit, "Polymers and Neutron Scattering", Oxford (1994)

L.S. Ornstein and F. Zernike, Phys. Z. 19, 134 (1918)

B. Zimm, J. Chem. Phys. 14, 164 (1946); 16, 1093 (1948)

X. 9. Questions

1. Does the interchain structure factor (with excluded volume) for dilute polymer solution tend to increase or decrease the scattering?
2. If an incompressible binary polymer mixture is characterized by one (independent) structure factor, by how many structure factors can a compressible binary mixture be described?
3. What is the origin of monomer/monomer interactions in polymer mixtures?
4. How to determine the spinodal line in incompressible polymer blends?
5. Does a numerical solution of the integral equation (with a realistic closure relation) describe local packing adequately? How about a mean field analytical solution (using the mean spherical approximation)?
6. Can the scattering from a concentrated solution of spheres (colloidal suspension for example) be described as the product of a single-particle and an interparticle structure factors?
7. What is the origin of the sharp "diffraction spots" observed from oriented block copolymers with spherical morphology?
8. What would be the scattering pattern from an unoriented lamellar morphology?
9. Stiff (rod-like) polymers are characterized by orientational phase transitions beside the spinodal and binodal lines. Name the two best known transitions
10. Using the random phase approximation, work out the three structure factors for an incompressible mixture of a diblock copolymer A-B and a homopolymer C (see Hammouda, 1993 for example).

XI. TYPICAL SANS DATA FROM POLYMER SYSTEMS

There are two main areas of SANS research on polymers: homogeneous mixtures and phase separated systems. Whereas sophisticated theories (mean field RPA for example) exist for the interpretation of data from homogeneous polymers, most data analysis from multiphase systems is based on following trends from size and scaling information. Nonlinear least-squares fitting of the scattering data to models as well as standard plots are the main tools. Standard plots consist in assessing linear behaviors (when plotting functions of the intensity as functions of Q) in order to extract characteristic slopes and intercepts.

XI.1. Standard Plots

The Guinier plot involves Ln(I) vs Q^2 in order to obtain $R_g^2/3$ (R_g is the radius of gyration of the inhomogeneity) as slope ($Ln(I)=Ln(I_0)-Q^2Rg^2/3+...$). The radius of gyration represents the effective size of the scattering "particle" whether it is a domain or a polymer chain. Interparticle effects always contribute to R_g except at the infinite dilution limit (case of an isolated particle). The usefulness of this plot stems from the fact that the obtained particle size (R_g) is independent of the absolute intensity (I_0). Instrumental smearing as well as polydispersity and multiple scattering appear to decrease the effective R_g.

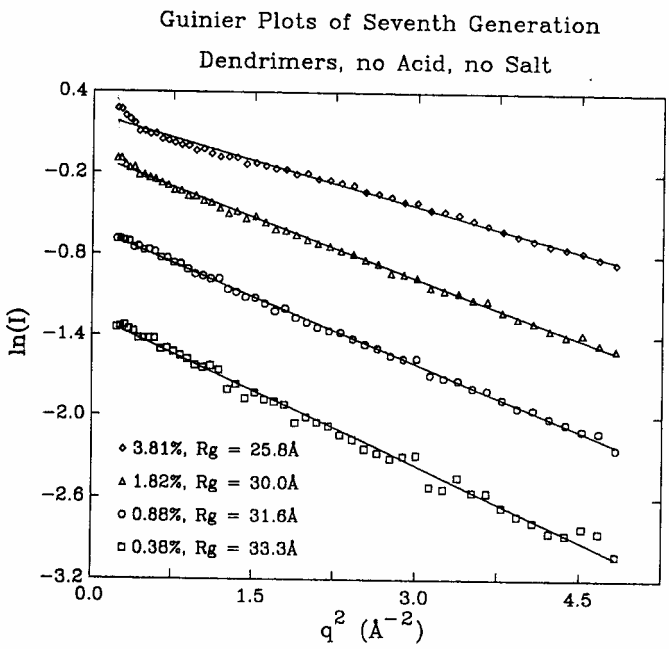

Figure XI.1: Guinier plot for a seventh-generation PAMAM dendrimer solution in heavy water at the concentrations noted on the figure and without neutralization (no added acid or salt). Dendrimers are highly regular gels that are grown outwardly from a central core; at each generation, the number of branches doubles. The obtained radius of gyration (extrapolation to zero concentration) is around 33A, which agrees well with the one provided by the supplier.

Another well known plot is the Zimm plot (1/I vs Q^2) which found wide use in light scattering from dilute polymer solutions where extrapolation to zero Q and zero concentration yields the molecular weight and the second virial coefficient. The Zimm plot is also useful in polymer blends (in the single-phase region) where the slope is proportional to the correlation length, which is proportional to the Flory-Huggins interaction parameter (incompressible RPA model). Assuming a Lorentzian form for the Q-dependence of the intensity: $I=I_0/(1+Q^2\xi^2)$ where ξ is the correlation length, a plot of 1/I vs Q^2 yields $1/I_0$ as intercept (call it A) and ξ^2/I_0 as slope (call it B). The correlation length is obtained as $(B/A)^{1/2}$. In the low-Q region, one can also expand $I=I_0(1-Q^2R_g^2/3+...) = I_0/(1+Q^2R_g^2/3+...)$, so that $\xi=R_g/(3)^{1/2}$. The Zimm plot is, however, useful beyond the low-Q region. In high-Q region, $Q^2\xi^2<1$ so that $1/I=Q^2\xi^2/I_0$. In this region, the single chain structure factor behaves as $2/Q^2R_g^2$ (high-Q expansion of the Debye function) so that $\xi=R_g/(2)^{1/2}$ is identified. In the case of polymer solutions with excluded volume interactions, the high-Q expansion is, instead, $2/(QR_g)^{1/\nu}$ where ν is the excluded volume exponent (ν=3/5 for fully swollen chains, ν=1/2 for theta chains and ν=1/3 for collapsed chains). Low-Q departure from linear behavior of the Zimm plot is a signature of non-homogeneity in the sample or of chain-branching.

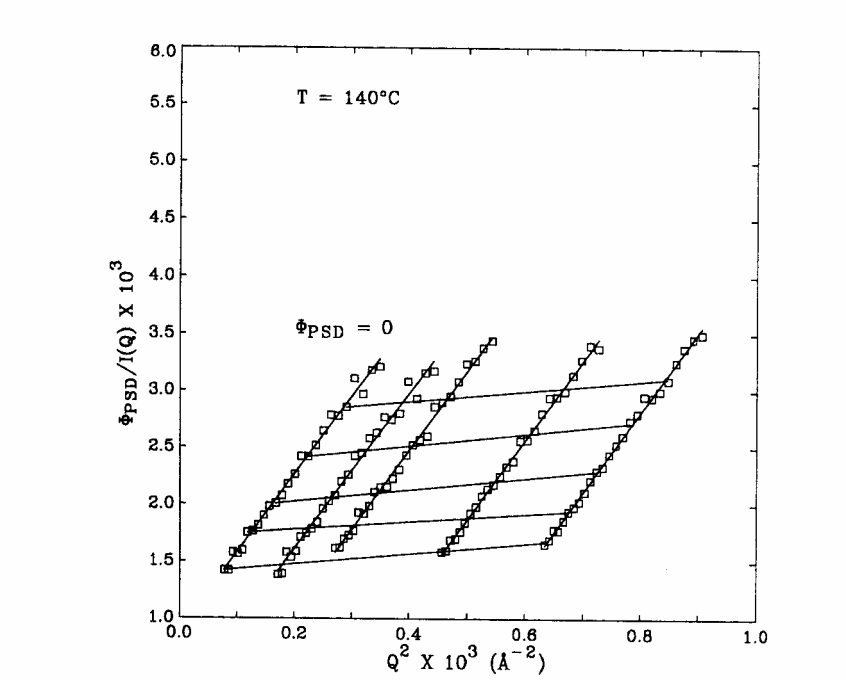

Figure XI.2: Standard Zimm plot for a deuterated polystyrene/polyvinylmethylether blend (M_W=1.88x10^5 and 3.98x10^5 g/mole respectively) mixture for four dilute polystyrene volume fractions of 1%, 1.8%, 3.8% and 5.4% at a temperature of 140^{o}C. Extrapolation to zero volume fraction yielded a slope and intercept which gave the degree of polymerization for polystyrene and the radius of gyration respectively.

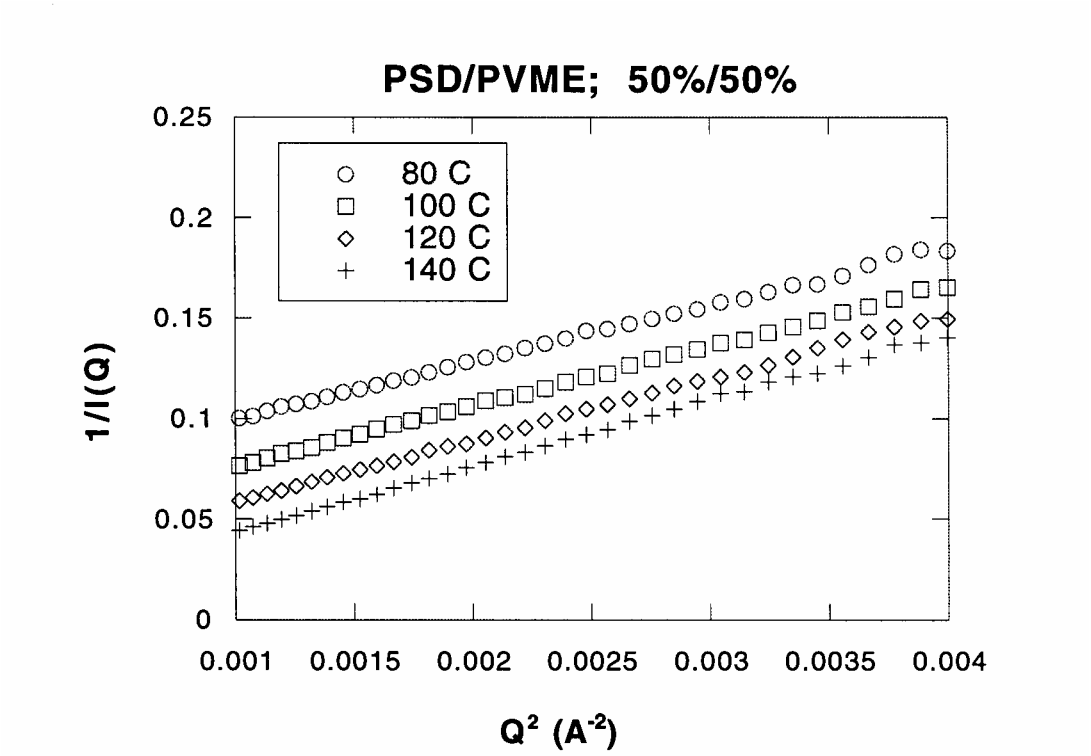

Figure XI.3: Zimm plot for a deuterated polystyrene/polyvinylmethylether blend mixture (M_W=1.88x10^5 and 2.01x10^5 g/mole respectively) at fixed composition (50%) and for various temperatures. The slope and intercept give a measure of the correlation length ξ.

The Kratky plot (Q^2I vs Q) emphasizes the Gaussian nature of polymer chains. Because at high-Q, the structure factor for Gaussian chains goes as $2/Q^2R_g^2$, this plot tends to a horizontal asymptote. Interchain contributions affect only the constant multiplying this term and not the $1/Q^2$ scaling behavior. Deviation from a horizontal asymptotic behavior indicates a non-Gaussian characteristic for the scattering objects. For instance for rigid rods, this plot would go to a linearly increasing asymptote $Q^2I = A+BQ$ because the structure factor for a rod goes like 1/Q at high Q and one has to use a more natural Kratky plot for a rod (QI vs Q) in order to recover the horizontal asymptote.

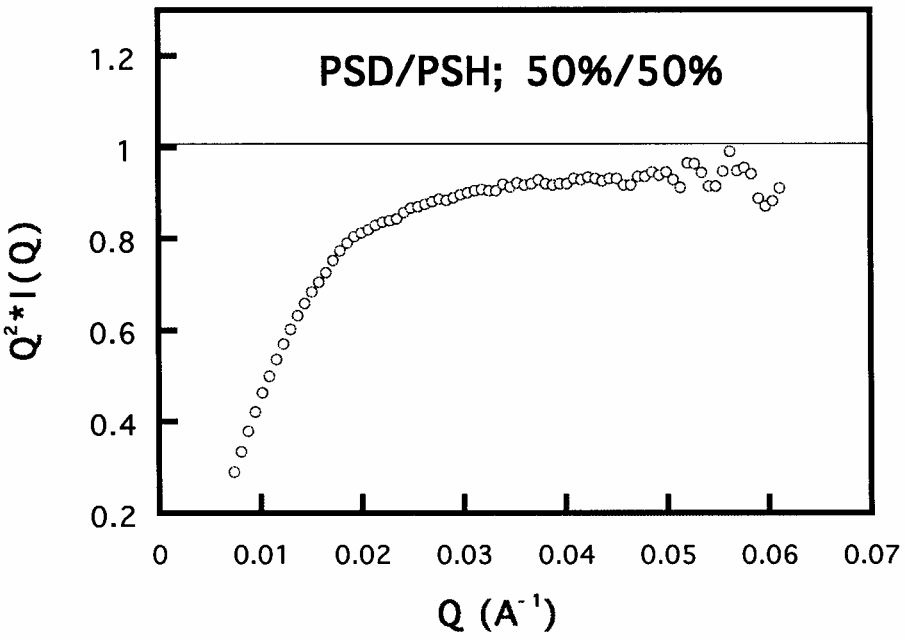

Figure XI.4: Kratky plot for a 50%/50% mixture of deuterated polystyrene and protonated polystyrene (M_W=174,000 and 195,000 g/mole respectively).

The manner in which the asymptote of a Kratky plot is reached yields information about chain branching. For instance, in a plot of Q^2I vs Q^{-2} ($Q^2I=A+B/Q^2$) the intercept B is related to the crosslink density in branched gels and networks (see Benoit et al, 1994).

The Porod plot (Ln(I) vs Ln(Q)) yields information about the so-called "fractal dimension" of the scattering objects. At high-Q, a slope of -2 is a signature of Gaussian chains in a dilute environment, whereas a slope of -1 points to rigid rods. A slope of -4 represents a smooth interface between domains in a multiphase system (Porod, 1951). Slopes between -3 and -4 characterize rough interfaces of fractal dimension D (Schmidt, 1988). Scattering from such a rough interface drops as $1/Q^{6-D}$. In the case of smooth interfaces, the scattered intensity at high Q goes like:

$$I(Q)\approx(CF)\phi(1-\phi)(2\pi S/VQ^4)$$

where S/V is the surface-to-volume ratio, ϕ is the inhomogeneities' volume fraction and (CF) is the contrast factor $(CF)=(b_A/v_A-b_B/v_B)^2$. This is a general result independent of the actual shape of the scattering particles (spheres, rods, etc). The origin of this result goes back to the form of the pair correlation function which can be written (for low interdistances r) as (see eqs. IX. 45-47 for example):

$$p(r) = p_0(r)[1-Sr/4V+...]$$

where $p_0(r)$ is the value at r=0. The structure factor is the Fourier transform:

$$I(Q) = (CF)\ \phi(1-\phi)V\ (1/R) \int dr\ p(r) \int_0^{\infty} \sin(Qr)/Qr]$$

which, at high-Q, goes to the limit mentioned above.

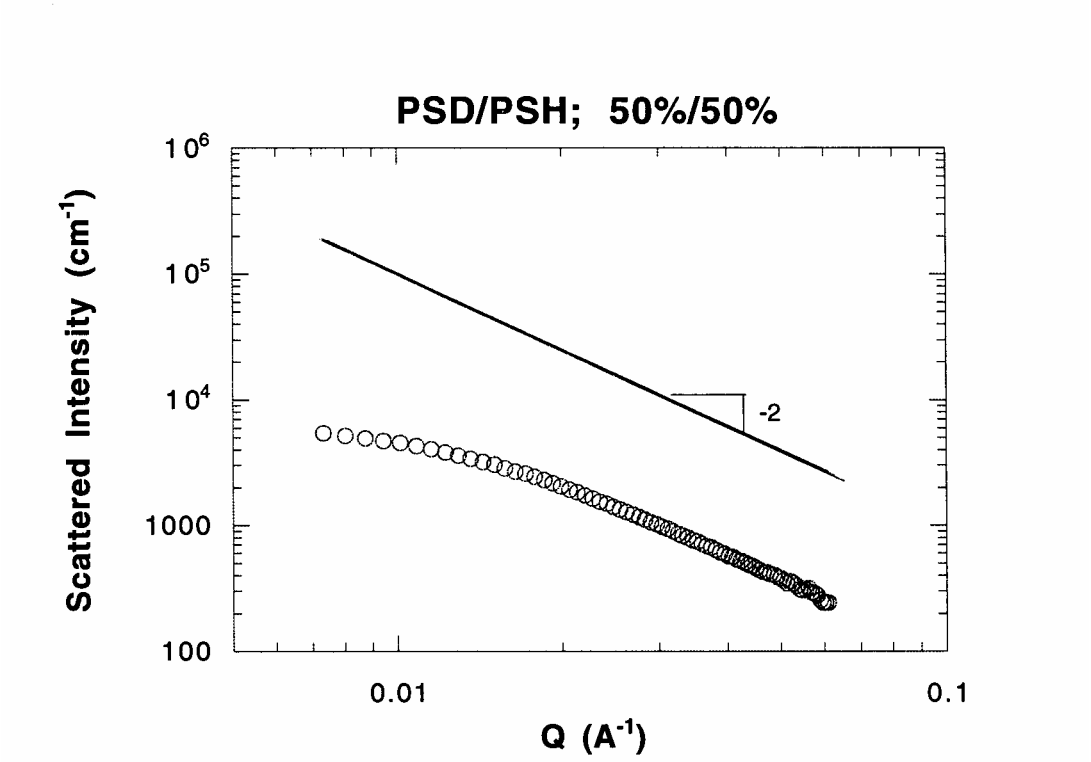

Figure XI.5: Porod plot for a blend of 50%/50% deuterated polystyrene and protonated polystyrene (M_W=174,000 and 195,000 g/mole respectively) measured at room temperature. The -2 slope is characteristic of Gaussian chains.

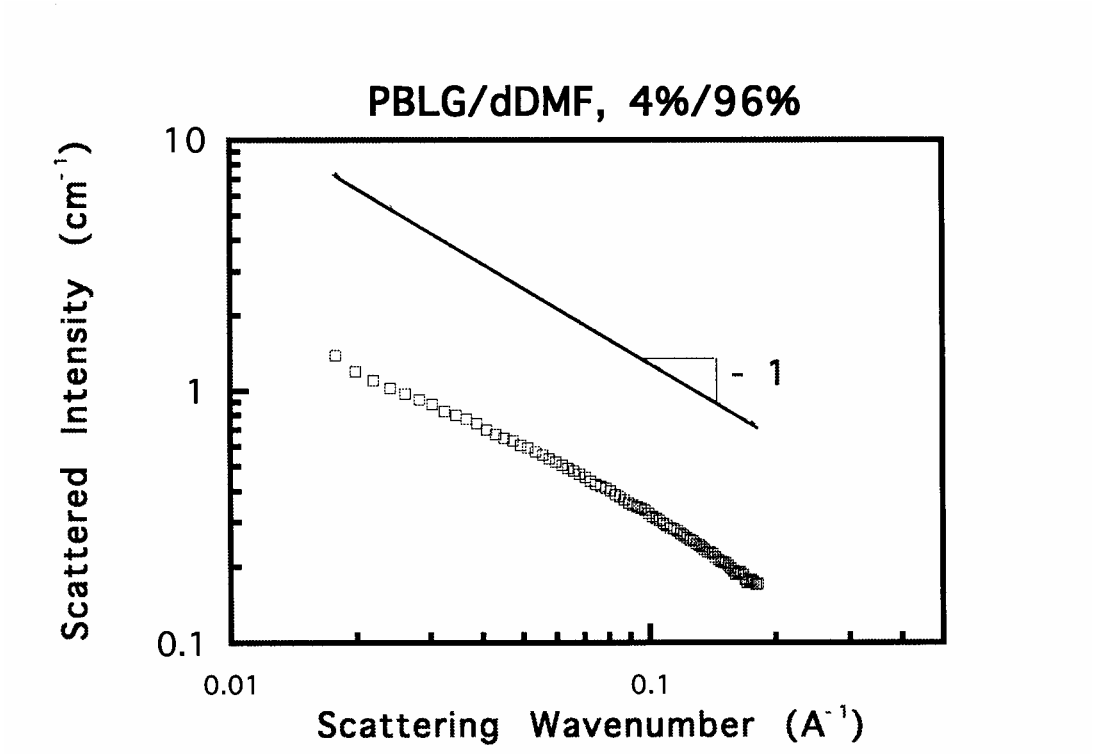

Figure XI.6: Porod plot for a solution of polybutyl-L-glutamate in deuterated dimethyl formamide solution (4% polymer). Because this is a liquid crystal polymer, scattering at high Q tends that of a rigid-rod with a -1 Porod slope.

XI.2. Typical Isotropic SANS Spectra from Polymer Systems

A number of SANS spectra will be described here in order to show the variety of possibilities and to give a "taste" of what typical scattering is encountered in polymer research.

The majority of SANS spectra follow a monotonic decreasing function of Q; for this reason these "all look alike". The Fourier transform is also a monotonically decreasing function of Q which is characteristic of correlation decay beyond a "correlation length". In the example of Figure XI.7, scattering intensity is seen to increase as composition fluctuations build up close to the spinodal transition temperature. Because the polystyrene/polyvinylmethylether blend system has a Lower Critical Spinodal Temperature (LCST), the scattered intensity increases upon heating of the sample.

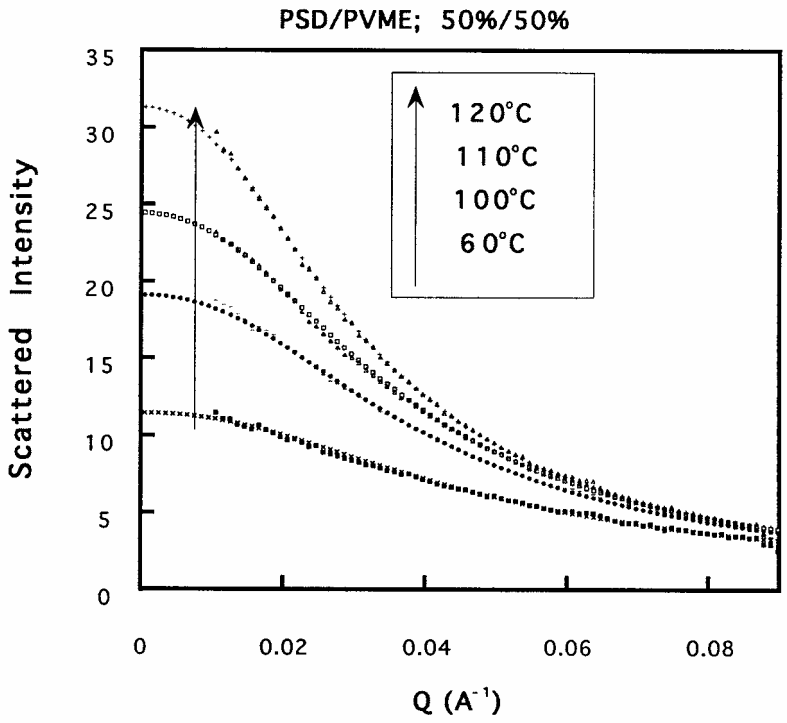

Figure XI.7: Typical SANS spectrum from a 50%/50% deuterated polystyrene/ polyvinylmethylether blend (M_W=1.95x10^5 and 1.59x10^5 g/mole respectively) for a number of temperatures approaching the spinodal decomposition temperature. Fits to the incompressible RPA formula and its extrapolation to zero-Q are also shown.

Diblock copolymers form various microstructures depending on the relative amount of one block with respect to the other. The three main morphologies consist of spherical, cylindrical or lamellar domains for block compositions between 0% and 17%, 17% and 32% or 32% and 50% respectively. Scattering models involving single-particle and interparticle contributions are useful for the interpretation of scattering data (domain sizes and interdistances). Other morphologies (double diamond, gyroid, etc) have also been discussed in the literature. Because of this microphase separation, scattering from block copolymers is characterized by a peak (a ring for isotropic scattering). The peak position (Q_{max}) gives an estimate of the average distance between domains ($d=2\pi/Q_{max}$).

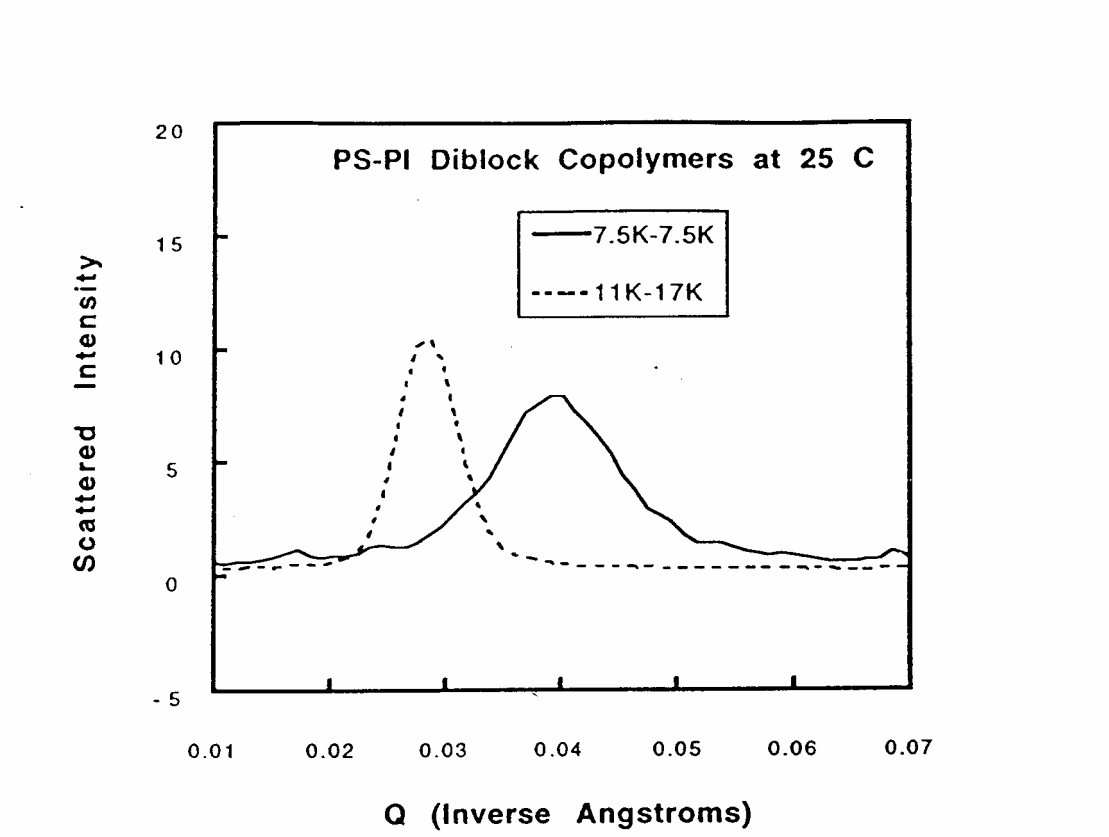

Figure XI.8: Scattering from two separate polystyrene/polyisoprene diblock copolymers of different compositions ($7.5x10^3$-$7.5x10^3$ and $11x10^3$-$17x10^3$ g/mole respectively). Both diblocks correspond to lamellar morphology with interdomain spacings of d=157 A and 217 A respectively.

Scattering from diblock copolymers is characterized by a peak even in the homogeneous one-phase region; the so-called correlation hole peak. Because the polystyrene-polyisoprene diblocks considered here are characterized by an upper order-disorder transition (ODT) temperature, the one-phase region is reached upon heating (note that for copolymers, the spinodal line is referred to as ODT). As the sample is heated through the ODT, the scattering peak becomes broader and moves slightly to higher Q values. Precise monitoring of the peak position and height give an estimate of the ODT temperature.

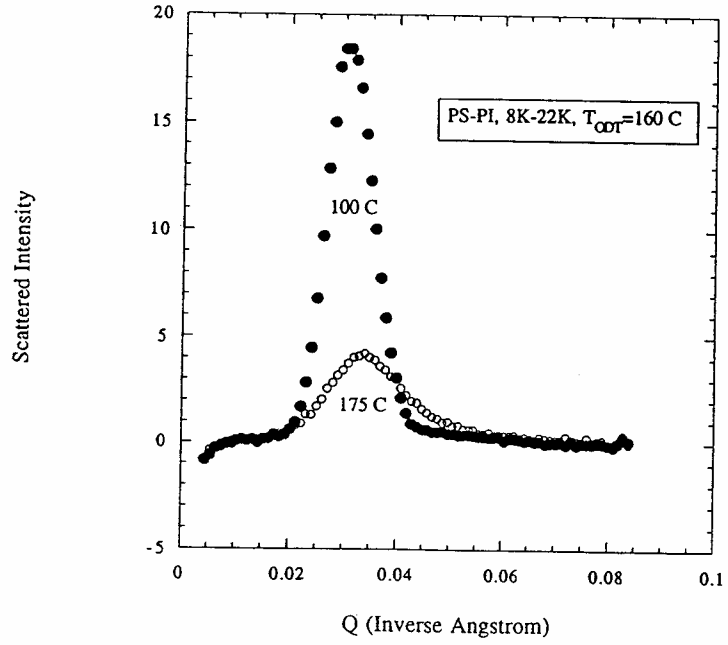

Figure XI.9: Scattering from a polystyrene/polyisoprene diblock copolymer (M_W=8x10^3-22x10^3 corresponding to cylindrical morphology) below and above the order-disorder temperature (T_{ODT}=160^{o}C).

Another example of diblock copolymer scattering corresponds to the scattering from a diblock in the spherical morphology. The first and second peaks can be clearly observed along with the hint of another higher order feature. For spherical morphology, if the first order peak occurs at Q_{max}, the second, third, etc., order peaks occur at (2)$^{1/2}Q_{max}$, (3)$^{1/2}$Qmax, (4)$^{1/2}$Qmax, etc. Note that for highly ordered cylindrical morphologies, these ratios are 1, (3)$^{1/2}$, (4)$^{1/2}$, etc., whereas for lamellar morphology, they are simply 1, 2, 3, etc.

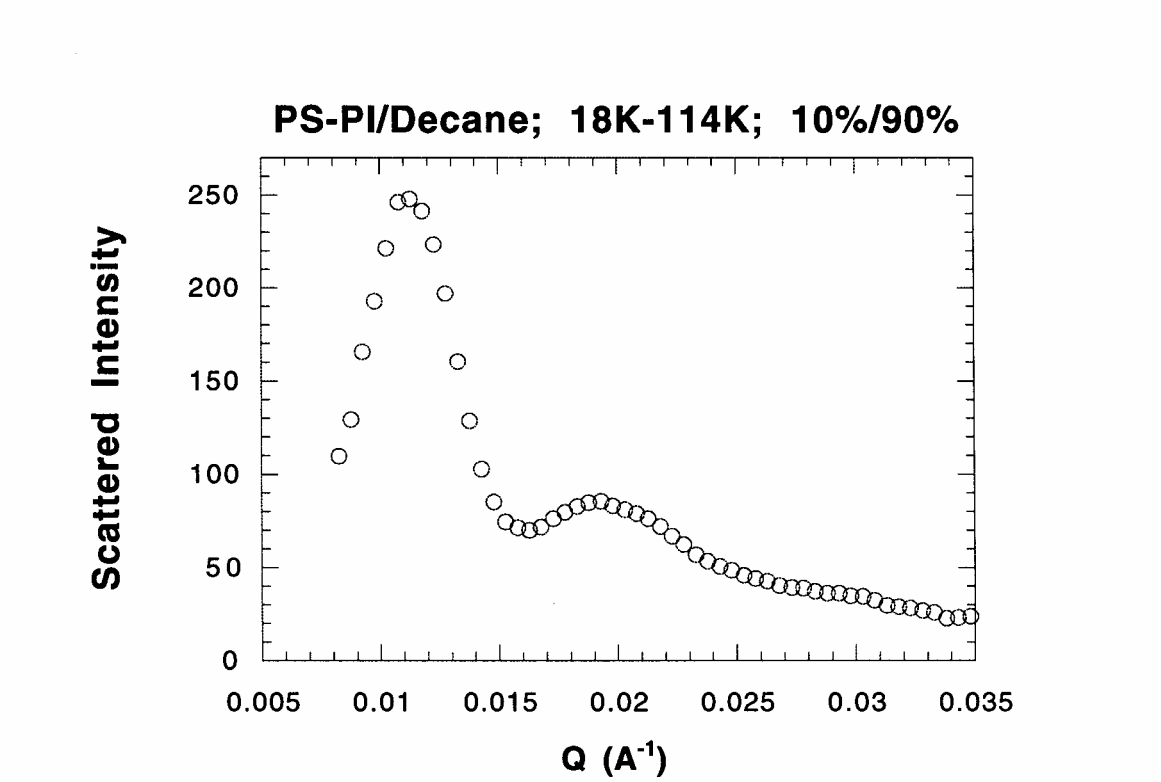

Figure XI.10: Scattering from a polystyrene-polyisoprene diblock copolymer with M_W=18 K-114 K dissolved in decane (10% copolymer) at room temperature.

The next example (polystyrene latex spheres in heavy water solution) is usually classified as a colloid (not a polymer) but is included here as an interesting example of sphere scattering. The Log(Intensity) vs Q variation shows the characteristic oscillatory behavior; the dips are not as sharp as predicted (see Figure IX.4) due to instrumental smearing.

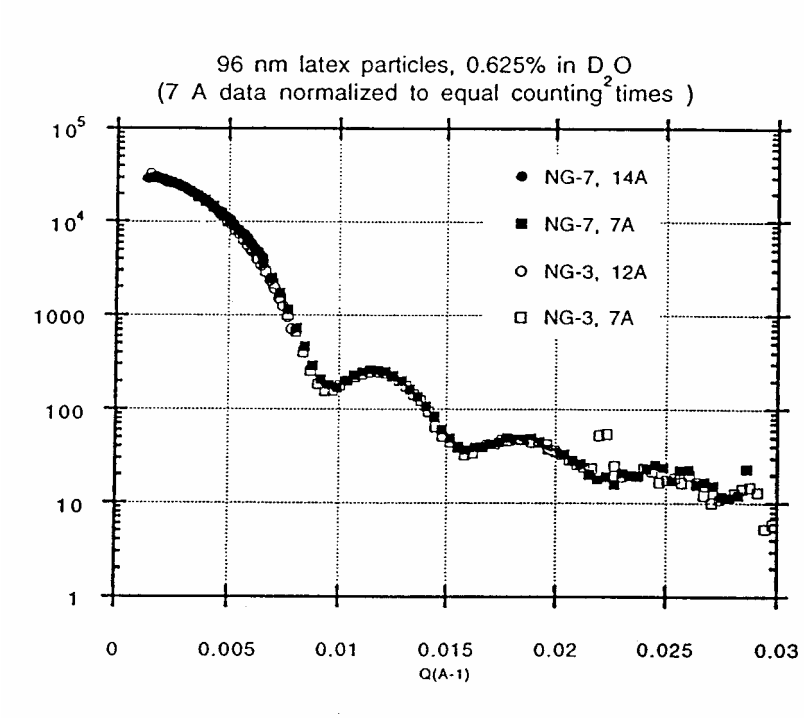

Figure XI.11: Scattering from a dilute (0.625% by weight) solution of polystyrene latex spheres in heavy water. From the first dip (minimum), a spheres radius can be measured (R=470 A); this value is seen to agree with the supplier estimate (480 A).

XI.3. Some Interesting Anisotropic Patterns from Oriented Polymer Systems

A few examples of anisotropic patterns from oriented polymer systems are presented here in order to show the wide diversity of SANS research.

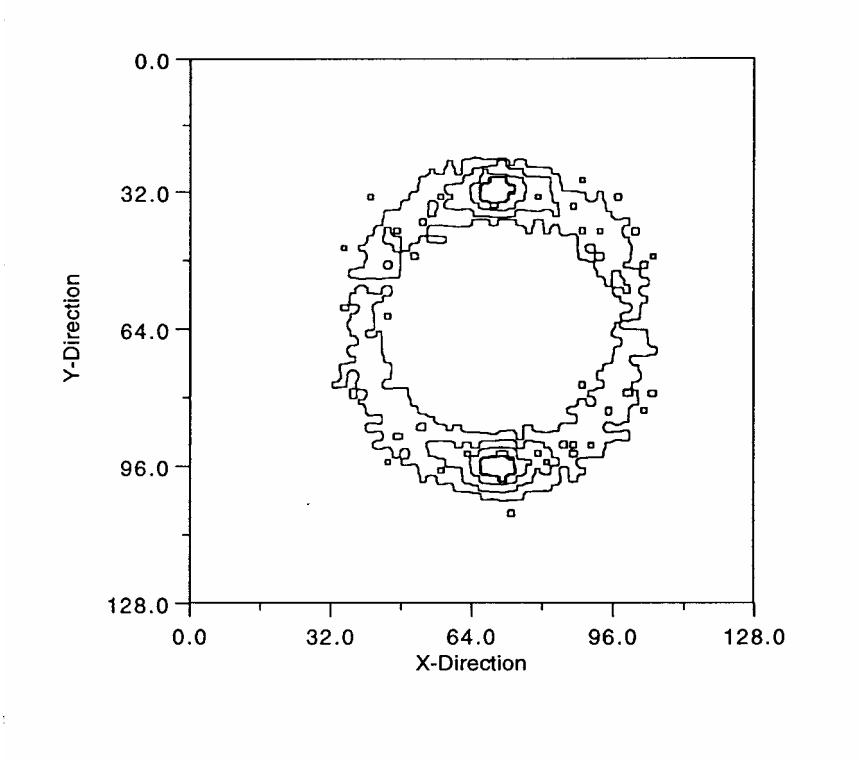

Figure XI.12: Scattering pattern from a polystyrene-polyisoprene diblock copolymer (M_W=11 K-17 K) dissolved in dioctyl phthlate (65% copolymer) and Couette sheared at a shear rate of 0.2 s^{-1}. The lamellar morphology is seen to orient under shear (scattering ring weakens and bright spots show up)

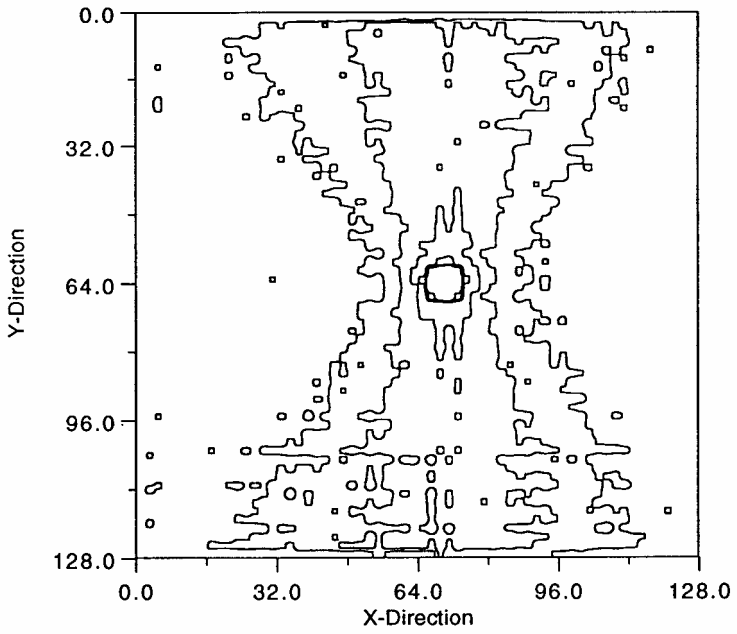

Figure XI.13: Scattering pattern from polybutyl-L-glutamate (a liquid crystal polymer) in deuterated dimethyl formamide solution (16% polymer) oriented in a 1 Tesla horizontal magnetic field. This is referred to as the "hourglass" pattern.

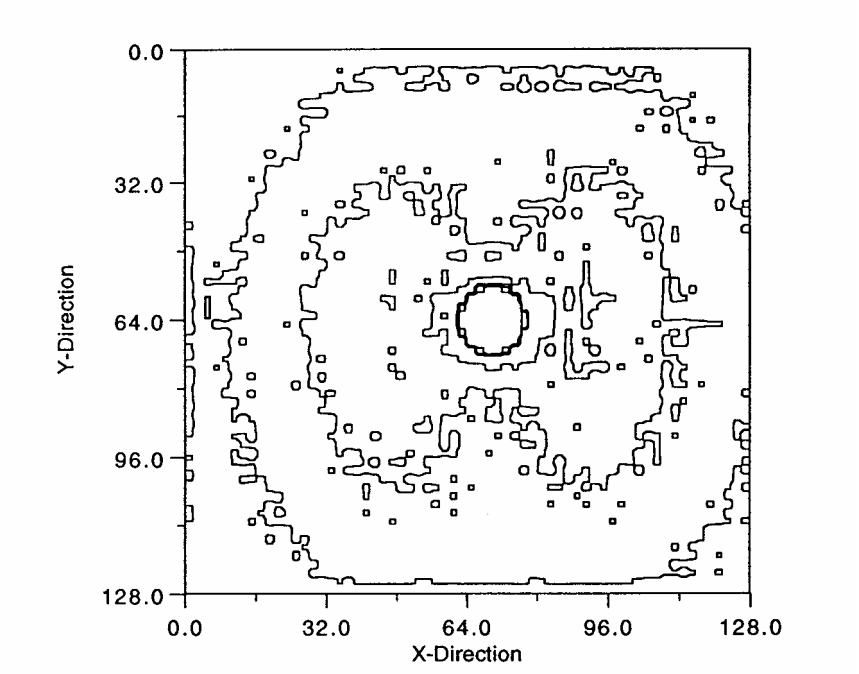

Figure XI.14: Scattering from a network of short (M_n=3,000) deuterated polydimethyl siloxane chains and long (Mn=25,000) protonated polydimethyl siloxane chains with relative compositions 25%/75% and stretched to a stretch ratio of 1.84. Note that the anisotropic pattern axis of symmetry is along the stretch direction (horizontal). This is referred to as the "butterfly pattern" because of its shape.

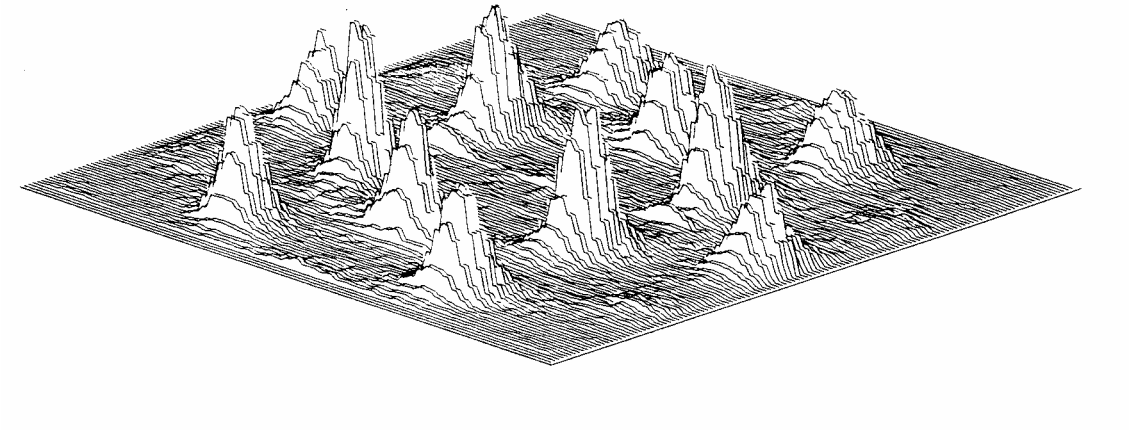

Figure XI.15: Polystyrene-polyisoprene diblock copolymer (Mw=44 K-22 K) in decane (17.5% polymer) under Couette shear at a shear rate of 3900 s^{-1}. Because decane is a specific solvent for polyisoprene, polymer micelles are formed. These form a regular lattice which orders into a

"perfect single-crystal" characterized by hexagonal symmetry. This is referred to as the "bright night sky" pattern.

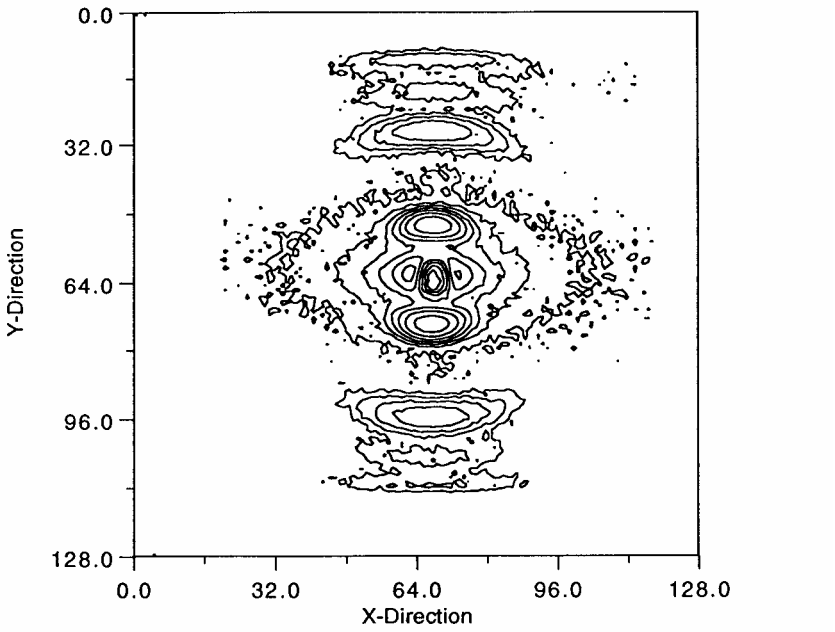

Figure XI.16: Scattering pattern from highly ordered biopolymer (collagen from a kangaroo tail tendon) showing the strong first and third reflection peaks as well as the weak fourth and fifth reflection peaks; the second reflection peak is not allowed. The ordered structure is along the fibers and has a d-spacing of 667 A.

References

H. Benoit, J.F. Joanny, G. Hadziioannou and B. Hammouda, Macromolecules 26, 5790 (1993)

G. Porod, Kolloid Z. 124, 83 (1951)

P.W. Schmidt, Makromol. Chem., Makromol. Symp. 15, 153 (1988)

XI.4. Questions

1. Do scattering inhomogeneities have to be spherical for a radius of gyration to be defined and measured through a Guinier plot?
2. Why are Zimm plots linear?
3. What is the use of a Kratky plot?
4. What information could be obtained by using a Porod plot for smooth interfaces?
5. Why does scattering increase when a phase transition line is approached?
6. What is the correlation hole effect in block copolymers?
7. Why does the block copolymer peak broaden when the one-phase region is entered?
8. Why is the axis of symmetry of a scattering pattern perpendicular to the orientation direction of the sample (except in the case of the butterfly pattern)?
9. When scattering contains bright peaks, why are peaks at high Q broader than peaks at low Q?

10. Thinks whether you could learn more about a sample of your research interests by aligning it (either though shear, rubbery stretch, or by applying a magnetic field).

XII. FINAL COMMENTS

The SANS technique has gained maturity in polymer research. In the words of one of the founders of polymer science "neutron scattering is among the four greatest developments (lasers, NMR, computers and neutron scattering) that made polymer science what it is today" (Prof. W.H. Stockmayer, Polymer Physics Gordon Conference, 1994). This technique has managed to grow steadily over the past twenty-five years from a "follow the trends" technique to a sophisticated characterization method in polymer morphology, thermodynamics, and rheology. Advances in the use of judicious sample environments (shear cells, magnets, pressure cells, temperature quench apparatuses, etc) have instilled new momentum. However, because neutron scattering is based at a few facilities only in the world, SANS is not as easily accessible as other method (NMR, light scattering, etc). Moreover, because SANS measurements are made in reciprocal space, other complementary techniques (such as microscopy) are often essential in order to obtain a "complete picture". Future prospects look as bright as in the past.

ACKNOWLEDGMENTS/DISCLAIMER

This material is based upon activities supported by a National Science Foundation (NSF) grant to NIST (DMR-9122444). Identification of certain equipment or materials does not imply recommendation by the National Institute of Standards and Technology. Help from the following scientists either through discussions or by contributing a figure is greatly appreciated: N. Balsara, B. Bauer, A. Gast, C. Glinka, R. Oeser, P. Thiyagarajan, N. Wagner.

REVIEW ARTICLES ON "SANS FROM POLYMERS"

"Scattering, Deformation and Fracture in Polymers", Materials Research Society Symposia Proceedings, Volume 79 (1987). Even though these proceedings did not focus on SANS, many SANS investigations were included.

G.D. Wignall, "Neutron Scattering", in Encyclopedia of Polymer Science and Engineering 10, Wiley (1987), G. Wignall, "Combined SANS and SAXS Studies from Polymers", Adv. X-Ray Anal. 36, 355 (1993), G. Wignall and F. Bates, "Neutron Scattering in Materials Science: SANS Studies of Polymers", MRS Bull. 15, 73 (1990)

J. Higgins and A. Maconnachie, "Neutron Scattering from Polymers", Meth. Exp. Phys. 23, 287 (1987)

R. Ullman, "SANS of Polymers", Polym. News 13, 42 (1987)

"International Conference on Small Angle Scattering", Special Issue of J. of Appl. Cryst., Vol. 21, No 6, (1988). A few review articles on SANS from polymers and microemulsions appeared in this issue. For instance: F.S. Bates, "SANS from Amorphous Polymers", J. Appl. Cryst. 21, 681 (1988), and S. Chen, E. Kalus and H. Hoffman, "SANS Investigation of Correlations in Charged Macromolecular and Supramolecular Solutions", J. Appl. Cryst. 21, 751 (1988).

R.W. Richards, "SANS Studies of Polymers: Selected Aspects", J. Macromol. Sci., Chem. A26, 787 (1989), R. Richards, "SANS from Interpenetrating Networks", Makromol. Chem., Macromol.

Symp. 40, 209 (1990), R. Richards, "SANS from Multiphase Polymers", Mol. Cryst. Liq. Cryst. 180A, 55 (1990), R.W. Richards, "SANS and NR in Polymer Characterization", Polym. Charact. 222 (1993)

R. Ottewill," SANS on Polymer Colloids", NATO ASI Ser. C303, 349 (1990)

R. Stein, "SANS Studies of Polymer Orientation and Phase Separation", Mol. Cryst. Liq. Cryst. 180A, 119 (1990)

L. Sperling, J. An M. Chang and D. Thomas, "Interpenetrating Polymer Networks", Int. Symp. Polym. Adv. Technol. 635 (1987), L. Sperling, "Recent Applications of SANS to Multicomponent Polymer Systems", Polym. Mater. Sci. 59, 150 (1988), L. Sperling, A. Klein, J. Yoo, K. Kim and N. Mohammadi, "The Utilization of SANS to Solve Polymer Latex Structural Problems: Basic Science and Engineering", Polym. Adv. Technol. 1, 263 (1990)

B. Crist, "Polymer Self-Diffusion Measurements by SANS", J. Non-Cryst. Solids 131, 709 (1991)

L. Auvray, "Contrast Methods in SANS. Applications to Polymer Systems", Proc. Int. Schl Phys. "Enrico Fermi", 114, 371 (1992)

T. Springer, "Recent Contributions of Neutron Scattering for Condensed Matter Research: Polymers", Phys. Scr. 11 (1993). This article is in a conference proceeding.

B. Hammouda, Sk. Krueger and C. Glinka, "SANS at the National Institute of Standards and Technology", J. Res. NIST 98, 31 (1993), B. Hammouda, "SANS from Homogeneous Polymer Mixtures: a Unified Overview", Adv. Polym. Sci. 106 (87 (1993)

T. Lodge, "Characterization of Polymer Materials by Scattering Techniques, with Applications to Block Copolymers", Mikrochim. Acta 116, 1 (1994).

F. Hardouin, N. Leroux, P. Keller, M. Mauzac and M. Achard, "SANS Studies on Side-on Fixed Liquid Crystal Polymers", Mol. Cryst. Liq. Cryst. Sci. Technol. A254, 267 (1994). This is a general review article with an emphasis on liquid crystal polymers.

B. Bauer and R. Briber, "The Effect of Crosslink Density on Phase Separation in Interpenetrating Polymer Networks", Adv. Interpenetrating Polym. Networks 4, 45 (1994). This is a review article with an emphasis on polymer networks.